

## **Small On-Board Environmental Diagnostic Sensors Package (SOBEDS)**

**Robert H. Redus  
Alan C. Huber  
Phil G. D'Entremont**

**John O. McGarity  
David J. Sperry  
Josef Dalcomo**

**Marilyn R. Oberhardt  
John A. Pantazis  
Scott J. Moran**

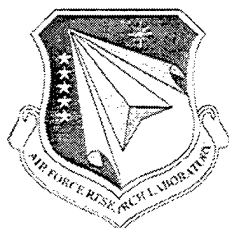
**AMPTEK, Inc.  
6 DeAngelo Drive  
Bedford, MA 01730**

**7 March 2000**

**Scientific Report No. 4**

**20010720 042**

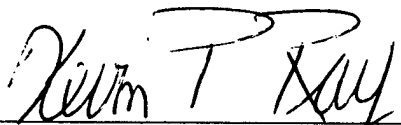
<b>APPROVED FOR PUBLIC RELEASE; DISTRIBUTION IS UNLIMITED.</b>
--



**AIR FORCE RESEARCH LABORATORY  
Space Vehicles Directorate  
29 Randolph Rd  
AIR FORCE MATERIEL COMMAND  
Hanscom AFB, MA 01731-3010**

---

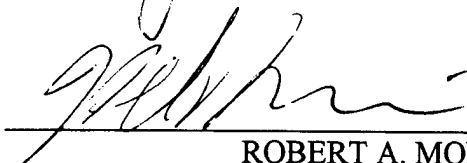
"This technical report has been reviewed and is approved for publication"



KEVIN P. RAY  
Contract Manager



GREGORY P. GINET  
Chief, Space Weather Center of Excellence



ROBERT A. MORRIS  
Chief, Battlespace Environment Division

This report has been reviewed by the ESC Public Affairs (PA) and is releasable to the National Technical Information Service (NTIS)

Qualified requesters may obtain additional copies from the Defense Technical Information Center (DTIC). All others should apply to the National Technical Information Service (NTIS)

If your address has changed, if you wish to be removed from the mailing list, or if the addressee is no longer employed by your organization, please notify AFRL/VSOS-IM, 29 Randolph Road, Hanscom AFB, MA 01731-3010. This will assist us in maintaining a current mailing list.

Do not return copies of this report unless contractual obligations or notices on a specific document require that it be returned.

REPORT DOCUMENTATION PAGE					Form Approved OMB No. 0704-0188	
The public reporting burden for this collection of information is estimated to average 1 hour per response, including the time for reviewing instructions, searching existing data sources, gathering and maintaining the data needed, and completing and reviewing the collection of information. Send comments regarding this burden estimate or any other aspect of this collection of information, including suggestions for reducing the burden, to Department of Defense, Washington Headquarters Services, Directorate for Information Operations and Reports (0704-0188), 1215 Jefferson Davis Highway, Suite 1204, Arlington, VA 22202-4302. Respondents should be aware that notwithstanding any other provision of law, no person shall be subject to any penalty for failing to comply with a collection of information if it does not display a currently valid OMB control number.						
PLEASE DO NOT RETURN YOUR FORM TO THE ABOVE ADDRESS.						
1. REPORT DATE (DD-MM-YYYY) 9 January, 2001		2. REPORT TYPE Scientific #4		3. DATES COVERED (From - To)		
4. TITLE AND SUBTITLE Small On-Board Environmental Diagnostic Sensor Package (SOBEDS)				5a. CONTRACT NUMBER F19628-95-C-0227		
				5b. GRANT NUMBER		
				5c. PROGRAM ELEMENT NUMBER 63401F		
6. AUTHOR(S) Robert Redus, Alan C. Huber, Phil G. D'Entremont, John O. McGarity, David J. Sperry, Josef Dalcomo, Marilyn R. Oberhardt, John A. Pantazis, and Scott J. Moran				5d. PROJECT NUMBER 2822		
				5e. TASK NUMBER GC		
				5f. WORK UNIT NUMBER AM		
7. PERFORMING ORGANIZATION NAME(S) AND ADDRESS(ES) Amptek Inc. 6 DeAngelo Drive Bedford, MA. 01730				8. PERFORMING ORGANIZATION REPORT NUMBER		
9. SPONSORING/MONITORING AGENCY NAME(S) AND ADDRESS(ES) Air Force Research Laboratory Space Vehicles Directorate 29 Randolph Rd. Hanscom AFB, MA 01731-3010 Contract Manager Kevin Ray/VSBS				10. SPONSOR/MONITOR'S ACRONYM(S) AFRL		
				11. SPONSOR/MONITOR'S REPORT NUMBER(S) AFRL-VS-TR-2000-1584		
12. DISTRIBUTION/AVAILABILITY STATEMENT Approved for public Release; Distribution unlimited.						
13. SUPPLEMENTARY NOTES						
14. ABSTRACT This report contains the summary of the scientific and engineering work performed as part of the development of the High Energy Proton instrument (HEP) and of the Low Energy Particle and Dosimetry instrument (LEPDOS). These instruments are part of the SOBEDS suite of instruments being developed by Amptek, Inc. The purpose of the HEP instrument is to measure the energy spectrum of energetic protons, specifically to obtain a differential spectrum for $25 < E < 440$ MeV and integral counts for $E > 440$ MeV. The purpose of the LEPDOS instrument is to measure: 1) the lower energy protons and electrons which may cause spacecraft anomalies, specifically protons from 0.7 to 80 MeV and electrons from 5 to $>250$ keV, 2) the dose and dose rate experienced by spacecraft electronics, 3) particles causing single event effects, and 4) to provide real-time warnings to spacecraft and operators of environmental conditions likely to cause anomalies, such as surface charging and deep dielectric charging.						
15. SUBJECT TERMS  Spacecraft radiation measurement      Electrons      Protons      Dosimetry						
16. SECURITY CLASSIFICATION OF:			17. LIMITATION OF ABSTRACT  UU	18. NUMBER OF PAGES	19a. NAME OF RESPONSIBLE PERSON Donald H. Brautigam	
a. REPORT  U	b. ABSTRACT  U	c. THIS PAGE  U			19b. TELEPHONE NUMBER (include area code) (781) 377-3890	

# Table of Contents

<b>1</b>	<b>INTRODUCTION .....</b>	<b>1</b>
<b>2</b>	<b>HEP FLIGHT INSTRUMENT CONCEPT .....</b>	<b>2</b>
<b>3</b>	<b>HEP SENSOR HEAD RESPONSE TO PROTONS.....</b>	<b>5</b>
3.1	EXPERIMENTAL APPARATUS.....	6
3.2	BEAM DESCRIPTIONS .....	7
3.3	EXPERIMENTAL RESULTS.....	9
<b>4</b>	<b>DESIGN, FABRICATION, AND TESTING OF HEP DIGITAL ELECTRONICS.....</b>	<b>16</b>
4.1	DIGITAL SIGNAL PROCESSING DESIGN .....	16
4.2	DIGITAL SIGNAL PROCESSING TEST AND MEASUREMENT .....	20
4.3	CPU AND INTERFACE DESIGN .....	22
<b>5</b>	<b>DESIGN AND FABRICATION OF OTHER HEP COMPONENTS.....</b>	<b>23</b>
5.1	SENSORS .....	23
5.2	ANALOG ELECTRONICS.....	23
5.3	POWER SUPPLY .....	23
5.4	MECHANICAL DESIGN.....	24
<b>6</b>	<b>LEPDOS DESIGN AND FABRICATION .....</b>	<b>24</b>
6.1	DESIGN, FABRICATION, AND CALIBRATION OF STANDARD LEPDOS UNITS.....	24
6.2	DESIGN, FABRICATION, AND CALIBRATION OF LEPDOS WITH ESA.....	25

## Figures

<b>Figure 1.</b> Conceptual drawing of the HEP sensor geometry.....	2
<b>Figure 2.</b> Plot showing computed energy deposition in the HEP detectors.....	3
<b>Figure 3.</b> Plot showing the energy deposited in S2 versus S1 .....	3
<b>Figure 4.</b> Block diagram of the HEP Electronics.....	4
<b>Figure 5.</b> Block diagram of HEP experimental set-up .....	6
<b>Figure 6.</b> Beam configurations used to calibrate the HEP protoflight sensor head. ....	8
<b>Figure 7.</b> Time of flight spectrum measured at Brookhaven National Laboratory.....	9
<b>Figure 8.</b> Plot comparing the computed and measured response of the HEP scintillators. ....	10
<b>Figure 9.</b> Plot comparing the computed and measured response in the S1S2 plane.....	11
<b>Figure 10.</b> Plot comparing the computed and measured response of the HEP PIPS detectors...	11
<b>Figure 11.</b> Plot showing the expected distribution of energies deposited in S1 and S2. ....	13
<b>Figure 12.</b> Spectrum generated in the S1 scintillator by 110 MeV protons.....	14
<b>Figure 13.</b> Plot comparing the measured and computed off-axis response of HEP.....	15
<b>Figure 14.</b> Measure and simulated effects of nuclear interactions.....	16
<b>Figure 15.</b> Simplified block diagram of the HEP digital electronics.....	17
<b>Figure 16.</b> Block diagram of the spectrum processing logic.....	19
<b>Figure 17.</b> Timing diagram of the DSP circuitry .....	19
<b>Figure 18.</b> Plots showing the measured performance of the coincidence circuitry .....	20
<b>Figure 19.</b> Measured performance of the HEP scalers at count rates up to $10^6 \text{ sec}^{-1}$ . ....	21
<b>Figure 20.</b> Plot showing the measured effects of pulse pile-up in S1.....	22
<b>Figure 21.</b> Drawing and photograph of LEPDOS S/N 007, which includes an ESA.....	26
<b>Figure 22.</b> Plot showing the measured angular response of the ESA. ....	27
<b>Figure 23.</b> Plot showing measured performance of the ESA.....	27

## Tables

Table 1 Summary of scintillator calibration results.....	13
Table 2. HEP power estimate.....	24
Table 3. HEP mass estimate.....	24
Table 4. Measured energy bins boundaries and geometric factors for the LEPDOS ESA.....	28

## 1 INTRODUCTION

This report contains the summary of the scientific and engineering work performed as part of the development of the High Energy Proton instrument (HEP) and of the Low Energy Particle and Dosimetry instrument (LEPDOS). These instruments are part of the SOBEDS suite of instruments being developed by Amptek, Inc. The purpose of the HEP instrument is to measure the energy spectrum of energetic protons, specifically to obtain a differential spectrum for  $25 \leq E \leq 440$  MeV and integral counts for  $E > 440$  MeV. The purpose of the LEPDOS instrument is to measure: 1) the lower energy protons and electrons which may cause spacecraft anomalies, specifically protons from 0.7 to 80 MeV and electrons from 5 to  $>250$  keV, 2) the dose and dose rate experienced by spacecraft electronics, 3) particles causing single event effects, and 4) to provide real-time warnings to spacecraft and operators of environmental conditions likely to cause anomalies, such as surface charging and deep dielectric charging.

During the fourth year of the SOBEDS contract, the primary technical effort on HEP was devoted to (1) test and calibration of the protoflight sensor head and (2) design, manufacture, and testing of the HEP electronics box. In the fourth year, extensive calibrations were carried out, using the protoflight sensor head, which is identical to the flight sensor head, and the calibration data analyzed. Based on the results, the electronics box which contains the analog and digital processing hardware, interfaces, and power supplies were designed and prototypes were built and tested. Some flight hardware was fabricated. The design and testing of the digital signal processing hardware was central to this effort.

The primary technical effort on LEPDOS in this fourth year of the SOBEDS contract has been devoted to the design, fabrication, and testing of a flight LEPDOS instrument, S/N 007, which includes an electrostatic analyzer (ESA) to measure electrons with energy below the threshold of the standard LEPDOS sensors. Some effort has gone into completing two additional standard LEPDOS instruments.

## 2 HEP FLIGHT INSTRUMENT CONCEPT

The measurement of high energy protons represents a challenge due to their large range in matter (300 MeV protons have a range of 24 cm in aluminum) and to the fact that the rate of energy loss in matter is low and varies slowly with energy above 150 MeV. This measurement is particularly difficult in space, where a nearly isotropic distribution of penetrating protons exists and where minimal shielding mass may be flown, due to spacecraft mass limits.

The HEP instrument uses a combination of detectors, including two primary scintillators, a veto scintillator, and four solid state detectors, to identify in-aperture protons and to measure their energy. The configuration of the detectors has been arranged to permit a clean measurement of the energy of in-aperture protons with energies between 20 and 440 MeV in the presence of an intense flux of out-of-aperture high energy protons. A conceptual drawing of the HEP sensor is shown in Figure 1.

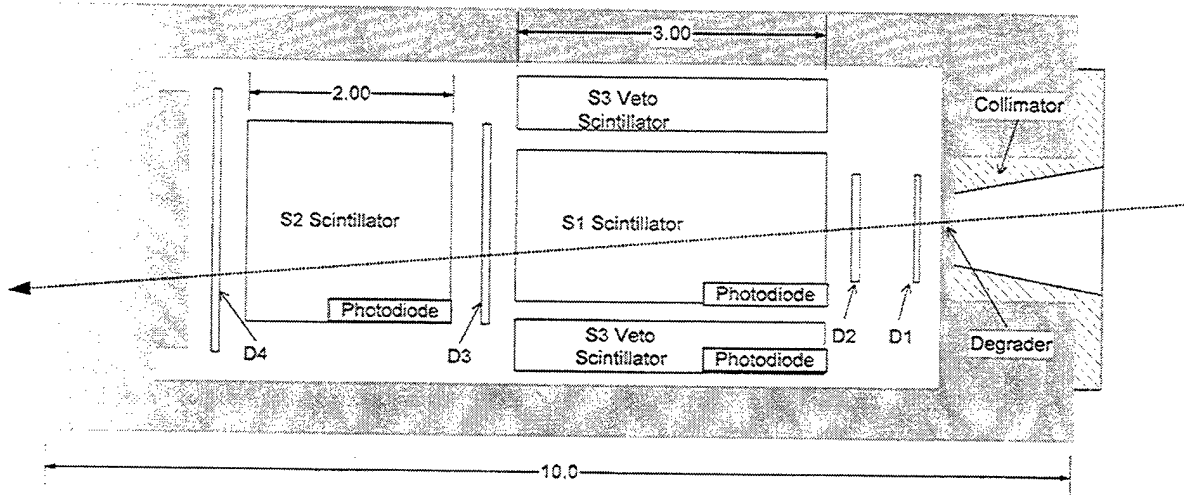


Figure 1. Conceptual Drawing of the HEP Sensor Geometry, Showing the S1 and S2 GSO Scintillators, the D1-D4 Si Diodes, the S3 Veto Scintillator, and the Shielding and Collimation.

Figure 2 and Figure 3 show calculated energy depositions in the detectors. In-aperture proton events are classified into three general types:

- Type A: proton traverses D1, D2 and stops in S1,
- Type B: proton traverses D1, D2, S1, D3 and stops in S2,
- Type C: proton traverses D1, D2, S1, D3, S2 and D4.

These in-aperture event types are caused by protons with different kinetic energies. Protons with energies both above the degrader threshold of 20 MeV and below 120 MeV will stop in S1 and produce Type A events. Type B events are caused by protons with energies between the 120 MeV and 175 MeV. Type C events are due to protons with energies above 175 MeV. Differential energy measurements for Type C events are made up to a proton energy of 440 MeV. Incident energies above 440 MeV will be measured in an integral channel. As shown in Figure 3, each incident proton energy corresponds to a unique combination of energy deposited in S1 and S2, denoted (S1,S2). There is a one-to-one mapping between points in the (S1,S2)

plane and incident proton energies. Since the S1 and S2 depositions are measured, this mapping is used to identify the energy of the incident protons.

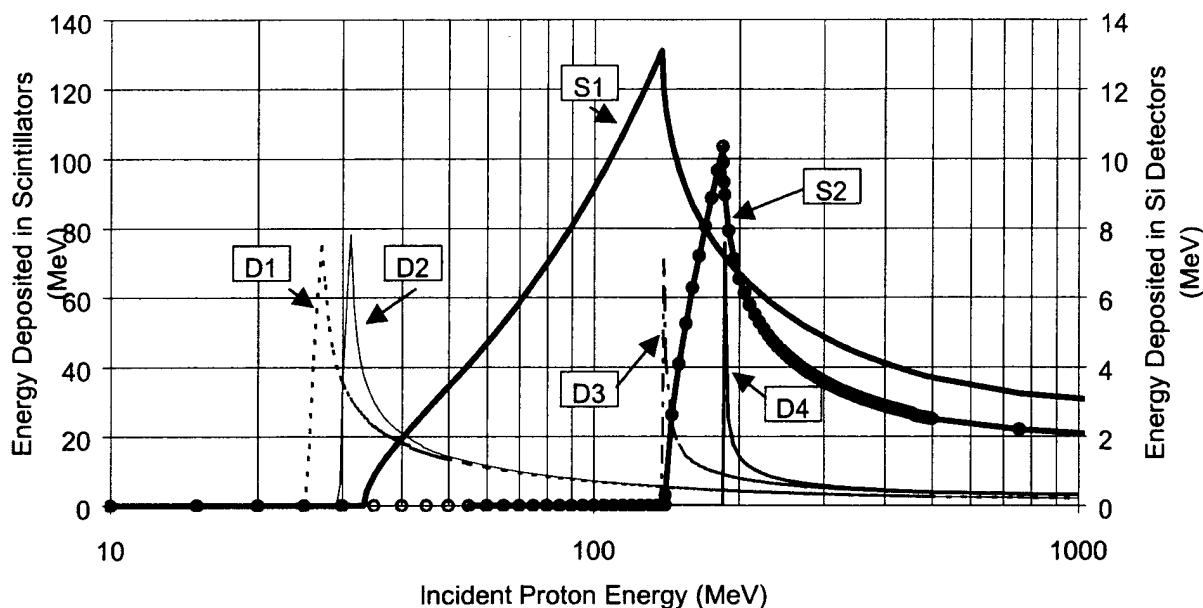


Figure 2. Plot Showing Computed Energy Deposition in the Six On-axis Detectors as a Function of Incident Proton Energy. Measuring the combination of the pattern of D detectors which are triggered, along with the amount of energy deposited in S1 and S2, permits accurate measurement of the incident proton energy.

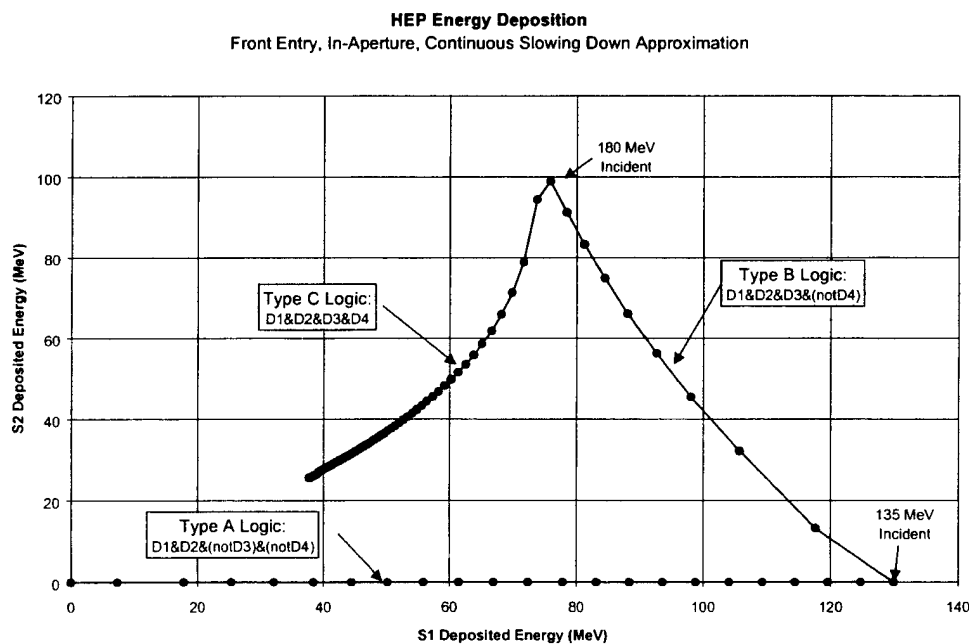


Figure 3. Plot Showing the Energy Deposited in S2 Versus S1, Along with the PIPS Detector Logic, as a Function of Incident Energy. This is the same data as is shown in Figure 2.



In addition to the three primary event types (A,B, and C), there can be many other interactions which must be considered in instrument design. Those of interest include responses caused by: 1) particles entering through the rear and passing through the aperture, 2) out-of-aperture protons penetrating the HEP collimator, 3) in-aperture protons undergoing nuclear interaction in HEP, and 4) random, accidental, simultaneous triggering of two or more detectors. These classes of events form a "background" which must be quantified to obtain an accurate knowledge of the incident spectrum. Their deposition pattern in the seven detectors differs from that of the primary event types. Designing the HEP data processing to make on-orbit measurements of these "background" event types, thus allowing measured corrections, has been a key part of the research and development effort and is essential to the success of this instrument.

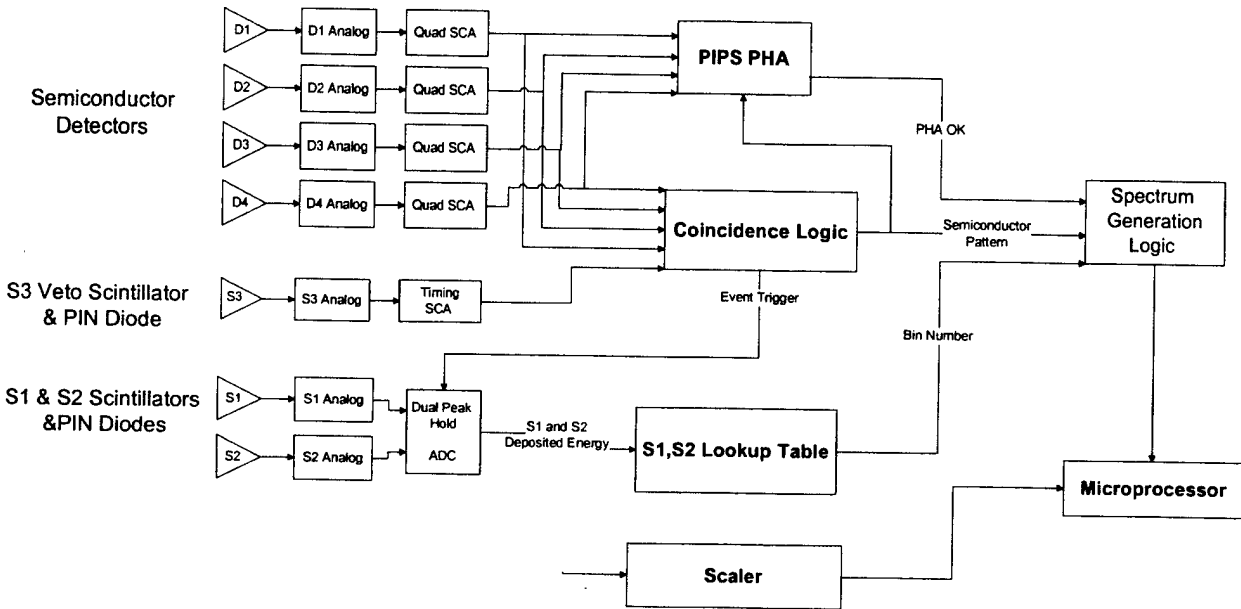


Figure 4. Block diagram of the HEP Electronics.

Figure 4 is a block diagram of the analog and digital electronics used in HEP. Each detector is connected to analog electronics to amplify and shape the output pulses. The outputs of the semiconductor detectors and the S3 veto scintillator go to discriminators, which trigger the coincidence logic. If these detectors match one of the predetermined patterns, within a 100 nsec coincidence window, then the S1 and S2 amplitudes are digitized. The coincidence logic accepts six patterns, termed "logic masks", set by ground command. Some pulse-height analysis is also performed on the outputs of the semiconductor detectors to reduce false triggering.

The digitized S1 and S2 energy depositions form a pair (S1, S2). Each portion of the (S1,S2) plane corresponds to one of 120 output data channels. Twenty-two of these are logarithmically spaced energy channels for front entry, in-aperture protons. They lie along the curve shown in Figure 3. The next twenty-six measure rear entry particles and background events. These do not have a one-to-one correlation with incident energy, so are "data" channels rather than "energy" channels. The final seventy-two are used in a calibration mode.

The digitized S1 and S2 values are compared with a look-up table containing the channel assignments. The combination of channel number, determined from the S1 and S2 values, and coincidence pattern, from the semiconductor detectors, is used by the Spectrum Generation

Logic to generate six 120-channel output spectra. The microprocessor reads a subset of these spectra, sums over the output data interval, log compresses them, and transmits them to the ground. The instrument has several operating modes, which determine the subset of the raw 6x120 array that is transmitted.

In the first two years of this program an engineering model (EM) of the HEP sensor head was manufactured for the purpose of testing the key hardware components and data handling algorithms intended for use with the flight instrument. The EM sensor head did not include any internal electronics. All signal processing and data acquisition were performed by external electronic modules, both custom designed and commercial NIM electronics. Using the EM, we performed extensive experimental and computational work to characterize the response of the HEP sensor head to protons. During the third year of the SOBEDS contract, the primary technical effort on HEP was devoted to the design and manufacture of the protoflight and flight HEP sensor heads. A model of the on-orbit instrument response was developed, and based on this and on results obtained previously with the EM, the instrument requirements were defined. The sensors were designed and manufactured. Certain portions of the analog electronics, located in the sensor head, were designed and flight hardware fabricated. By the end of the third year, initial testing of the protoflight sensor head was in progress.

During the most recent year, the fourth year, testing and calibration of the protoflight sensor head was completed and the data analyzed. Based on these experimental results some minor modifications were made to the sensor design and the flight sensor head fabricated. The electronics box, which includes the analog and digital signal processing electronics and the spacecraft interface, was designed and prototypes of most of the circuitry built and tested. As the fourth year ends, design of the flight electronics box is in progress.

### **3 HEP SENSOR HEAD RESPONSE TO PROTONS**

One of the most important tasks completed in the last year was a detailed measurement of the response of the protoflight sensor head to protons. The protoflight and flight sensor heads are identical. They differ only in that the unit designated as "protoflight" underwent much more extensive tests for design verification. The results obtained with the protoflight are directly applicable to the flight sensor head.

The most important measurements were conducted by the Amptek, Inc. staff and personnel from AFRL/VSBS at the Harvard Cyclotron during the last weekend of September, 1998 and at the Brookhaven National Laboratory AGS accelerator in October, 1998. The purpose of the work was to evaluate the performance of the HEP protoflight sensor head when exposed to in-aperture proton beams with energies between 20 and 2,000 MeV, to calibrate the instrument over this energy range, and to measure the response of the instrument to in-aperture protons experiencing nuclear interactions and to penetrating out-of-aperture protons.

### 3.1 EXPERIMENTAL APPARATUS

The experimental apparatus combined the protoflight sensor head (including sensors and preamplifiers) with a breadboard of the analog electronics and external electronic modules for digital signal processing. The use of external electronics permitted the work on the sensor head to proceed independently and in parallel to the work on the development of HEP digital electronics.

A block diagram of the electronics is shown in Figure 5. The goal of the electronics is to determine, on an event-by-event basis, the energy deposited in the seven detectors when a proton passes through the instrument. The primary electronic components are (1) the ADC, which digitizes the analog signals corresponding to deposited energy, and (2) the coincidence circuitry, which gates the ADC when a valid event has occurred. Additional components include a scaler, to measure the actual count rates, a time-of-flight telescope, to separate protons from the lighter particles produced at Brookhaven, a monitor detector, and a motion control system. The operation of the time-of-flight telescope was described in detail in the previous annual report.

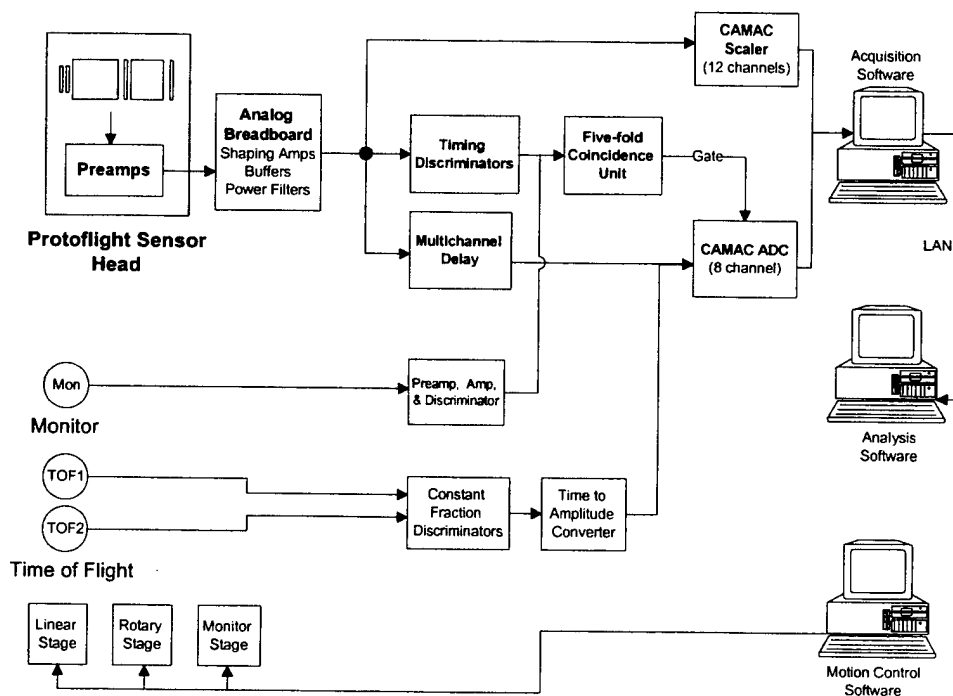


Figure 5. Block Diagram of Experimental Set-up Used to Measure the HEP Protoflight Sensor Response.

The protoflight sensor head contains, in addition to the sensors, preamplifiers and a portion of the shaping amplifier circuitry. The outputs of the sensor head were sent to a breadboard version of the analog board, containing the rest of the shaping amplifier circuitry. Because the external electronics were located outside of the beam line for personnel access, a distance of up to 100', the analog breadboard included buffer circuits, not intended for the flight boards, to drive the 100' coaxial cables.

The Analog Breadboard module produces seven shaped and amplified analog signals, proportional to the energy deposited in each of the seven detectors in the sensor head. There

were five inputs to the Coincidence module, which could be selected from among D1, D2, D3, D4, a beam monitor solid state detector and a time-of-flight (TOF) telescope signal. The Coincidence Model could be configured to accept any combination of these five signals, including single counts from any sensor, as a valid event. For a valid event, the Coincidence unit generated a logic signal which gated the CAMAC ADC. Unless a preset coincidence requirement was met the ADC did not digitize any signals. Once a valid event occurred, the ADC performed pulse height analysis on all (up to eight) of its input signals. The CAMAC scaler was used to count the beam induced events in all of the sensor head detectors (S1, S2, S3, D1, D2, D3 and D4), the beam monitor detector, and the TOF telescope. In addition, the total number of valid events, as determined by the Coincidence unit, was also counted.

The HEP beam experiments were controlled by a computer network. One computer ran the data acquisition program HEPDAQ, which communicated with the CAMAC crate using a SCSI card. HEPDAQ polled the CAMAC crate for valid events accepted by the ADC. If such an event (receipt of a gate from the Coincidence unit by the AD811) occurred, HEPDAQ would 1) transfer the digitized pulse height data for that event to the computer, 2) clear the old data from the ADC and 3) enable the ADC to accept the next event. After every 250 events processed by HEPDAQ, the program would read and clear the data from the scaler.

HEPDAQ stored the data retrieved on an event-by-event basis in a disk file. In order to free up the system resources for CAMAC communications, HEPDAQ performed no data analysis and was strictly a data retrieval and storage program. A second computer ran the data analysis and display program. This program would periodically access the data file written on the data acquisition computer by HEPDAQ, using a small local area network, perform simple analysis on the data and update the various displayed spectra and scaler counts.

A third computer ran another program that communicated with the motion control system using the PC-38 card, supplied by the motion system manufacturer. The motion control system included one rotary and two linear stages. The sensor head was mounted on top of the rotary stage, which in turn was attached to a linear stage. This configuration allowed the sensor head to be moved perpendicularly to the beam and rotated with respect to the beam axis. The solid state beam monitor detector was mounted on the second, independent linear stage (the Monitor Stage). This allowed the monitor to be placed in the beam line and directly upstream of the sensor head, whenever desired by the experimenter.

### **3.2 BEAM DESCRIPTIONS**

Figure 6 shows the configuration of the two beams where most of the data were obtained. The Harvard Cyclotron produces a 160 MeV proton beam. The beam exits the vacuum environment of the accelerator through a thin pressure window and enters the room where the experiment is performed. Just downstream of the window, the beam is directed through a 3.2 cm diameter collimator. Several calibrated degrader plugs (made of lead and Lexan) can be inserted into the collimator tunnel to decrease the incident beam energy. The standard degrader set produces the following mean energies at the exit of the collimator: 29, 37, 45, 54, 73, 92, 111, 131 and 149 MeV. In addition to lowering the mean energy, the degraders also cause additional spreading in energy due to straggling. The lowest energies are associated with the broadest distribution in energy incident on the instrument. The properties of the incident beam, the mean energies and the energy distribution, are well known from previous measurements [ref]. The sensor head was located 165 cm downstream of the collimator.

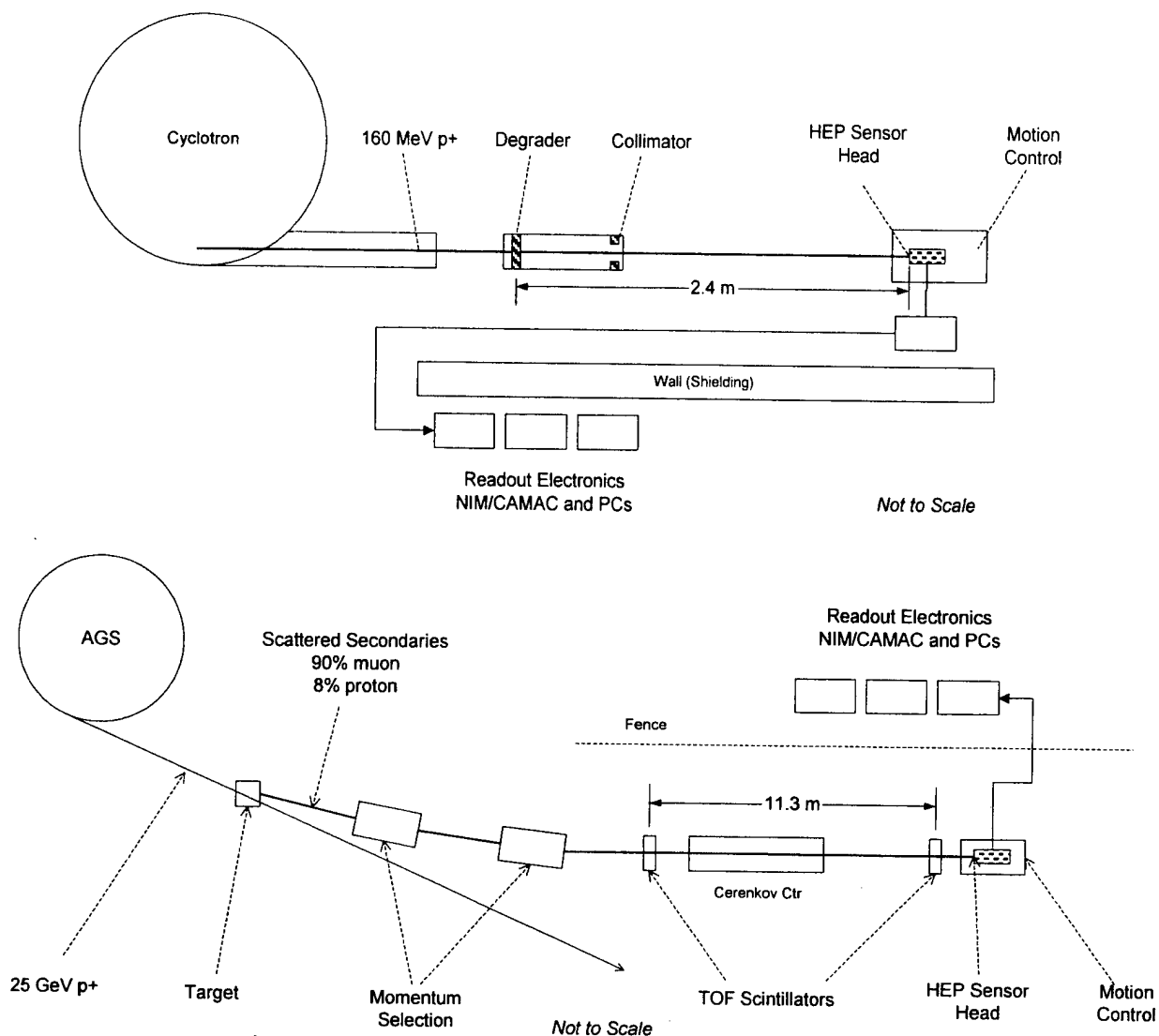


Figure 6. Beam Configurations Used to Calibrate the HEP Protoflight Sensor Head. The Harvard Cyclotron beam, shown on top, was used for energies from 20 to 160 MeV. The B2 Test Beam, from the Brookhaven AGS, was used for energies from 180 to over 2,000 MeV.

The AGS measurements were conducted at the B2 Test Beam. The AGS primary beam consists of 25 GeV protons, which are incident on a target. The B2 Test Beam consists of the secondary particles produced within this target and includes a variety of particles (muons, protons, positrons, pions, deuterons, tritons, and others) at a wide range of energies. A set of bending magnets and selection windows allows the user to select particles of a particular momentum. The kinetic energies and velocities of the particle species will differ, due to mass differences. To select particles of a given species, a time of flight (TOF) telescope was used to measure the velocity. Proton energies from 184 MeV to 2 GeV were used in the measurements reported here. This corresponds to  $\beta$  from 0.57 to 0.94, and with a TOF distance of 11 m, to transit times of 39 to 64 nsec. For muons at these momenta,  $\beta$  varies from 0.99 to 0.999 and thus to an essentially fixed transit time of 37 nsec.

The TOF telescope (loaned to us by the PHOENIX group at the AGS) consisted of two plastic scintillator detectors placed 11 m apart and located directly upstream of the sensor. The time difference between the particle passage through the front and back TOF detectors was converted to an analog voltage pulse using a constant fraction discrimination and a time-to-amplitude converter. The TOF signal was used to gate the coincidence logic, to trigger on only the proper species, and as an input to the ADC. This permitted us to directly measure the velocity, and hence energy, of each particle incident on the sensor.

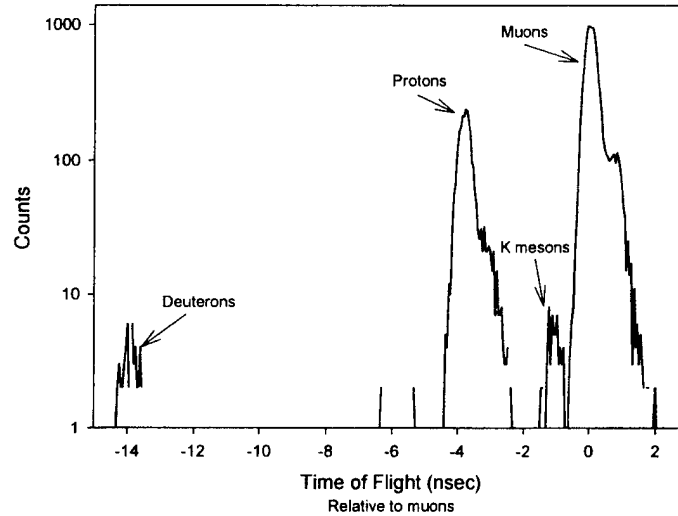


Figure 7. Time-of-Flight Spectrum Measured at Brookhaven National Laboratory's AGS B2 Test Beam at a Momentum of 2.0 GeV/c, Showing Beam Composition and the TOF Resolution.

**Figure 7** is a plot of the time of flight spectrum, showing the beam composition and indicating the operation of the TOF trigger. The data shown here were taken at a momentum of 2.0 GeV/c, which corresponds to a proton  $\beta$  of 0.90 and a proton kinetic energy of 1.27 GeV. The incident beam is predominantly light particles, which are indistinguishable at this timing resolution (positrons and  $\pi$  mesons have transit times within 90 picoseconds of the muons). K mesons have a theoretical transit time 1 nsec greater than the muons, protons 3.9 nsec, and deuterons 14 nsec. The proton peak has a width of 0.7 nsec FWHM. This includes spreading due to the distribution of incident momenta, admitted by the momentum windows, along with the timing jitter of the system

### 3.3 EXPERIMENTAL RESULTS

#### *Instrument Response*

Plots of the measured response of the instrument to the in-aperture incident protons are shown in Figure 8 and 9. Figure 8 compares the energy deposited in the S1 and S2 scintillators with that computed using the Janni model. Figure 9 shows the same data, but it shows the distribution in the S1S2 plane, and also shows the rear entry data. In both figures, the error bars represent the total measured FWHM of the peaks, which includes spreading due the width of the incident beam. The instrument response is much narrower. Figure 10 shows the PIPS data. In all cases, excellent agreement is found between the measurements and the model.

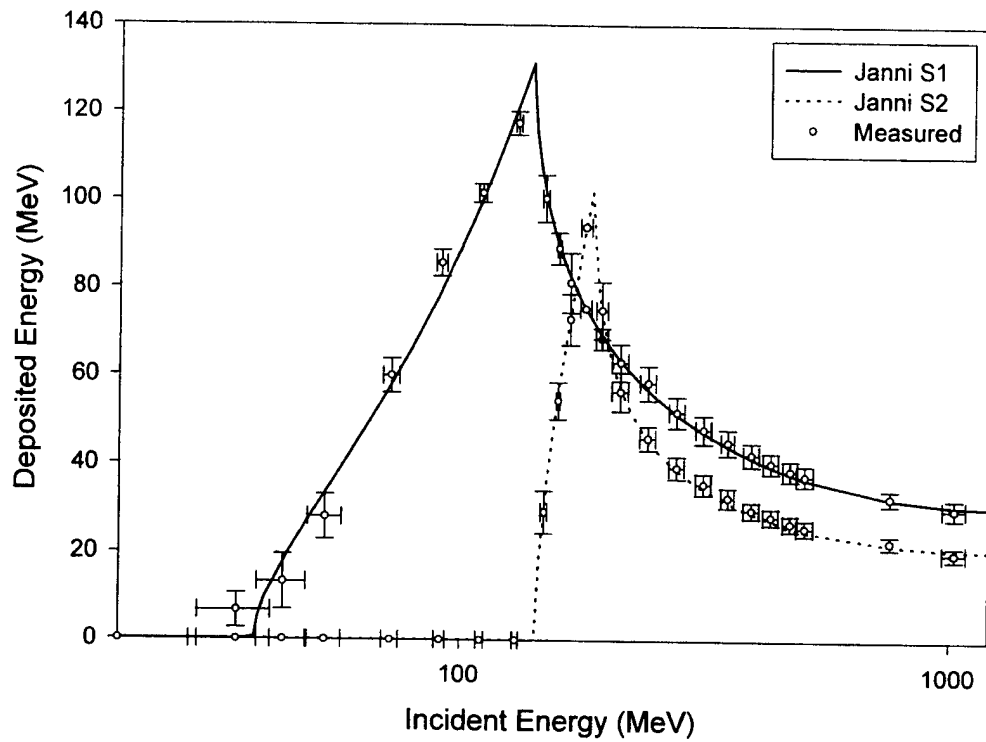


Figure 8. Plot Comparing the Computed Response of the HEP Scintillators to that Measured at Harvard and Brookhaven, Using the Protoflight Sensor Head, Identical to the Flight Sensor Head.

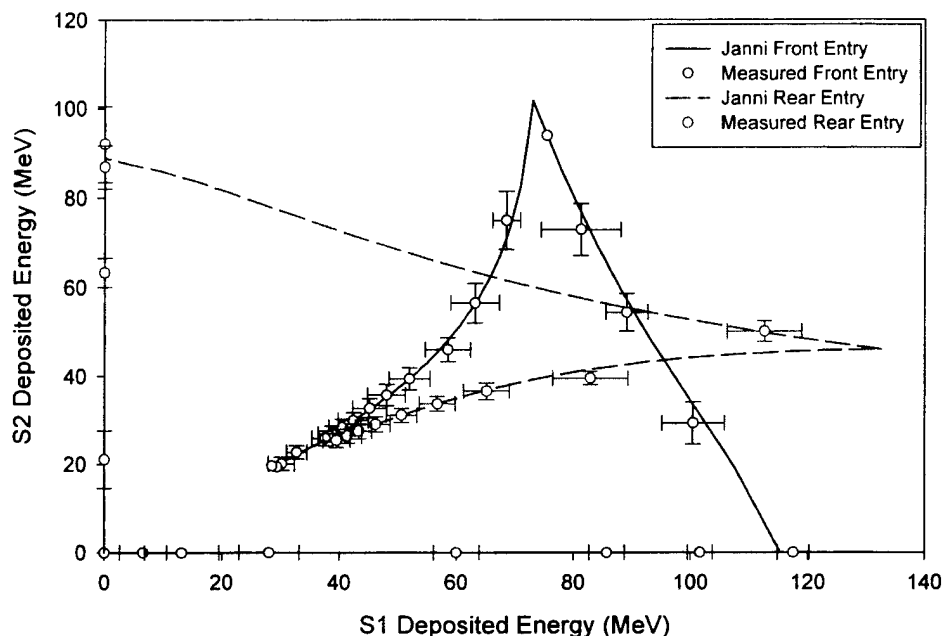


Figure 9. Plot Comparing the Computed and Measured Response in the S1S2 Plane, for Both Front and Rear Entry Protons.

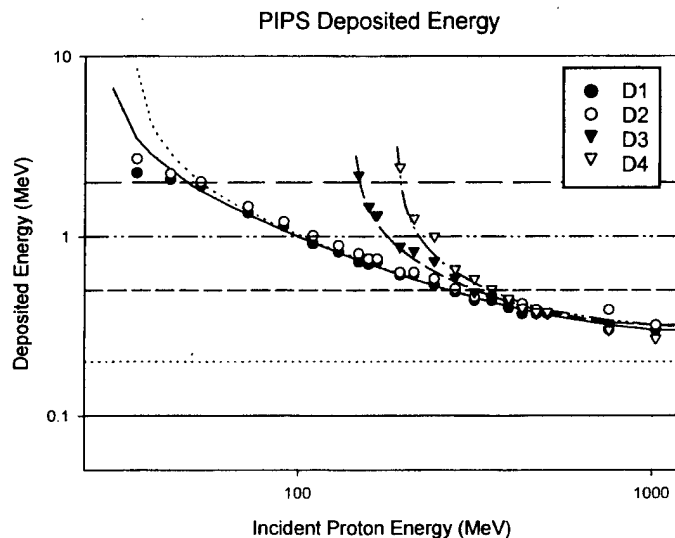


Figure 10. Plot Comparing the Computed Response of the HEP PIPS Detectors to that Measured at Harvard and Brookhaven.

To obtain the energy calibration for the detectors, all of the in-aperture front entry data above 50 MeV and the rear energy data above 110 MeV were used. For each experimental run, a histogram of counts versus channel number was generated. For each spectrum with a symmetric peak, the centroid channel was computed, while for asymmetric peaks the peak channel was selected. This was then compared with a detailed model of the expected energy deposition in the instrument, including all of the various layers in the instrument, including the minor layers of plastic and metal contacts. This model, discussed in the previous annual report, is based upon



the Janni results. The Janni model yielded deposited energy, for each case, while the experimental data yielded peak channels. A linear regression was performed between the computed depositions and the peak channels.

It was empirically determined that the best fit was obtained using a 3% correction to the Bragg-Kleeman rule used for estimating the stopping power of the GSO. As was discussed in the previous report, the Bragg-Kleeman rule is only valid to about 10%, so this correction is reasonable. Data taken previously with the Engineering Model indicated a 5% correction.

#### *Light Yield and Scintillator Resolution*

In addition to measuring the overall response, the properties of the scintillation detectors were measured, including the light yield, electronic noise, and total resolution. To obtain the light yield, the PIN photodiodes were exposed to gamma sources ( $^{137}\text{Cs}$ ,  $^{60}\text{Co}$ ) and the photopeaks and Compton edges measured. This provided an absolute calibration of the MCA output, in electron-hole pairs per channel. The calibration of the energy response described above provided the MeV deposited per channel. From these two, the number of electron-hole pairs per MeV was deduced. To obtain the electronic noise, a test pulser was used. Table 1 is a summary of the results.

Table 1 Summary of Scintillator Calibration Results

	Light Yield (elec.-hole pairs/MeV)	Electronic Noise (MeV FWHM)	Correlation Coeff.
S1	4,470	0.7	0.997
S2	4,740	0.6	0.999
S3	2,410	1.1	0.969

The energy resolution of the scintillators was measured to be approximately 3.0 MeV for S2 and 4.2 MeV for S1, at incident energies around 500 MeV. The electronic noise, 0.6 and 0.7 MeV respectively, is negligibly small since the peak broadening terms add in quadrature. Detailed analysis showed that the primary peak broadening term, for both scintillators, comes from the fluctuations in deposited energy due to the occasional production of higher energy secondary electrons. This is the mechanism behind the well-known Landau distribution for thin detectors. Depositions in the HEP scintillators for energies between 200 and 2000 MeV are described by the Vavilov distribution, which is intermediate between the high energy Landau distribution and the low energy gaussian. Figure 11 below is a computed plot of the energy deposited in the scintillators by a monoenergetic incident beam. The computation was based upon a published analytical approximation to the Vavilov distribution, and yields a full-width at half-maximum of 2.8 MeV in S2 and 3.5 MeV in S1. This is clearly the dominant term limiting the resolution of the scintillators.

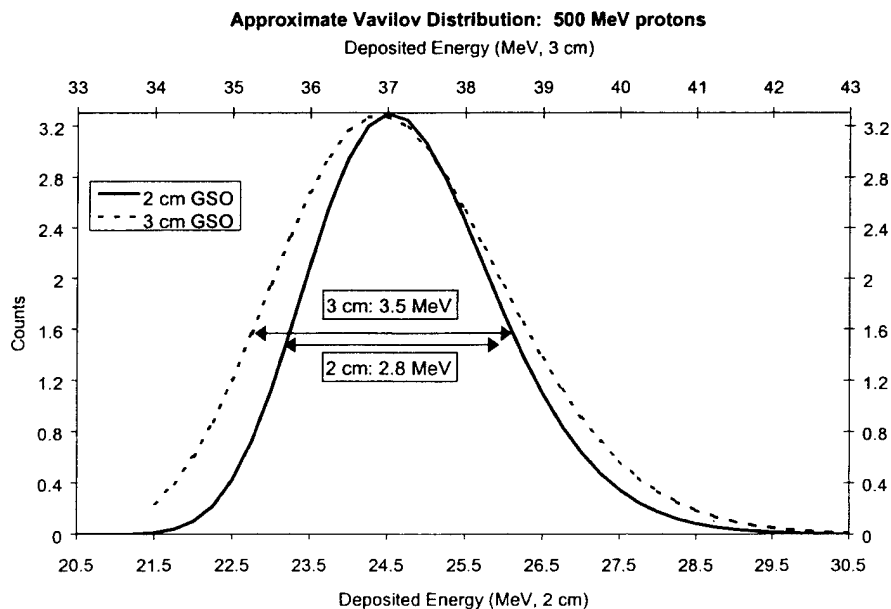


Figure 11. Plot Showing the Expected Distribution of Energies Deposited in the S1 and S2 Scintillators, for 500 MeV Incident Energy Protons. The spreading is due to Landau fluctuations in energy deposition.

In Figure 12, a spectrum measured using 110 MeV protons with the current protoflight sensor, using photodiode readouts and Spectralon reflectors, is compared with a spectrum

obtained previously using photomultipliers. This shows very clearly that the sensor and electronic design planned for the flight instrument do not degrade the total resolution relative to that obtained previously. In particular, the use of the PIN photodiodes instead of photomultipliers, the use of a fast shaping time to minimize pulse pile-up, and the detector geometry and light collection techniques had no measurable impact on resolution. The signal size, electronic noise, and signal to noise ratio were as expected for all detectors, including the S3 veto scintillator.

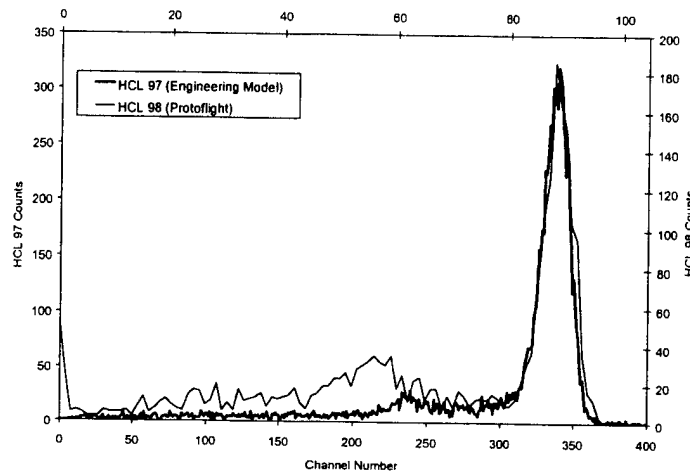


Figure 12. Spectrum Generated in the S1 Scintillator by 110 MeV Protons, Comparing the Response of the Protoflight Unit to that Obtained Previously Using the Engineering Model.

#### *Off-Axis Response*

The response of the instrument to off-axis penetrating protons was measured at the beam facilities. One important experimental result was the discovery that the electrically active area of the PIPS detectors was larger than expected. These detectors were designed for the measurement of  $\alpha$  particles, using mechanical collimation to restrict the area over which the  $\alpha$  particles are incident. This mechanical collimation determines the active area specified by the manufacturer, however the electrically active area is larger. For D1 and D2, the electrically active area is 50 mm<sup>2</sup> instead of 25 mm<sup>2</sup>, so this is significant. Since the energetic particles measured by HEP penetrate the collimation, the electrically active area is the relevant quantity. The HEP mechanical design was based upon the assumption that the specified active area was the true active area. With the "bonus" area, there are allowed trajectories that pass through the shielding and significantly degrade the response of the instrument to even on-axis particles.

To remedy this, custom ion-implanted detectors with the proper electrically active area were obtained from EG&G Ortec. These are passivated, ion-implanted silicon detectors from the Ultra™ series. They are circular, with an electrically active area of 25mm<sup>2</sup> and a depletion depth of 500  $\mu$ m. With these detectors, this particular problem should be resolved. The custom Ortec detectors were designed, fabricated, and underwent initial testing in the most recent year. They are now installed in the flight sensor head. The geometry will be verified in final beam tests.

Once the "bonus" area of the PIPS detectors is accounted for, the measured off-axis response of HEP is as expected. At sufficiently low energies, protons do not penetrate the shielding (130 MeV in front, 100 MeV in back, 60 MeV from the side). At sufficiently high energies, e.g. 300

MeV and up, protons incident along specific trajectories at about  $15^\circ$  off axis can pass through D1, D2, and S1 without striking S3 or D3. These cause false "A" events (which are defined by the pattern of D detectors triggered), with a deposited energy of about 30-70 MeV. This is as expected. Figure 13 compares the measured and calculated response of HEP to off-axis 330 MeV protons (these calculations took into account the bonus area). The in-aperture response has a half-angle of  $7^\circ$ , as expected. Penetrating protons just outside this cone can pass along the trajectory described above and indeed result in false "A" events. The response falls to zero between 20 and  $30^\circ$ . The angular and energy response of these events is in reasonable agreement with calculation results. The new D1 and D2 detectors should significantly reduce the off-axis response from that depicted here.

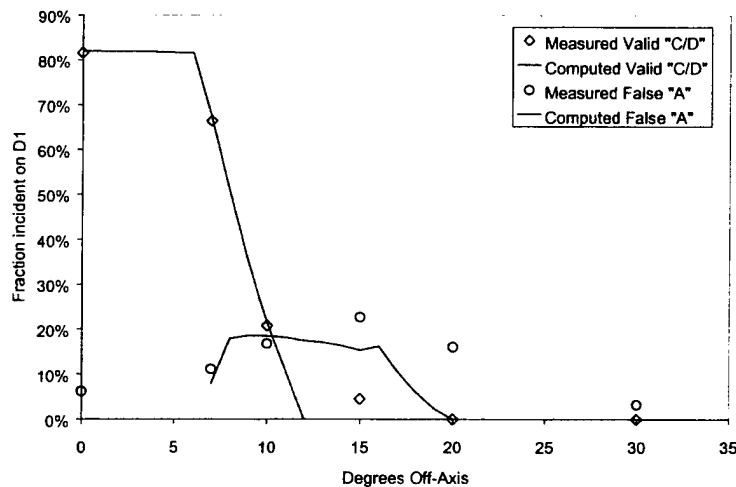


Figure 13. Plot Comparing the Measured and Computed Off-axis Response of HEP to 330 MeV Protons. Results are discussed in the text.

### *Nuclear Interactions*

As was discussed in the previous annual report, a considerable fraction of the protons measured by HEP will undergo inelastic nuclear scattering, i.e. nuclear interactions. The binding energy per nucleon is about 7 MeV, so the incident energy of the protons is more than enough to liberate nucleons from target nuclei. Simple analytical estimates indicate that on the order of 10% of the incident protons above 100 MeV will undergo nuclear interactions. When a nuclear interaction occurs, the pattern of energy deposition in the scintillators will differ from that predicted by the Janni model.

Figure 14 is a plot comparing the measured and computed effects of nuclear interactions on HEP. The computations were obtained from the LAHET code discussed in the previous annual report. The measured results were obtained at 250 MeV, at an energy where all four PIPS detectors should be triggered. On the left in Figure 14 is a scatter plot of the observed S1S2 pulse heights using events triggering D1, D2, D3 but not D4, which can only occur with a nuclear interaction. The simulation results were obtained with the same PIPS logic requirements. An empirical broadening of 3 MeV FWHM was added to the simulation result, to account for the finite scintillator resolution.

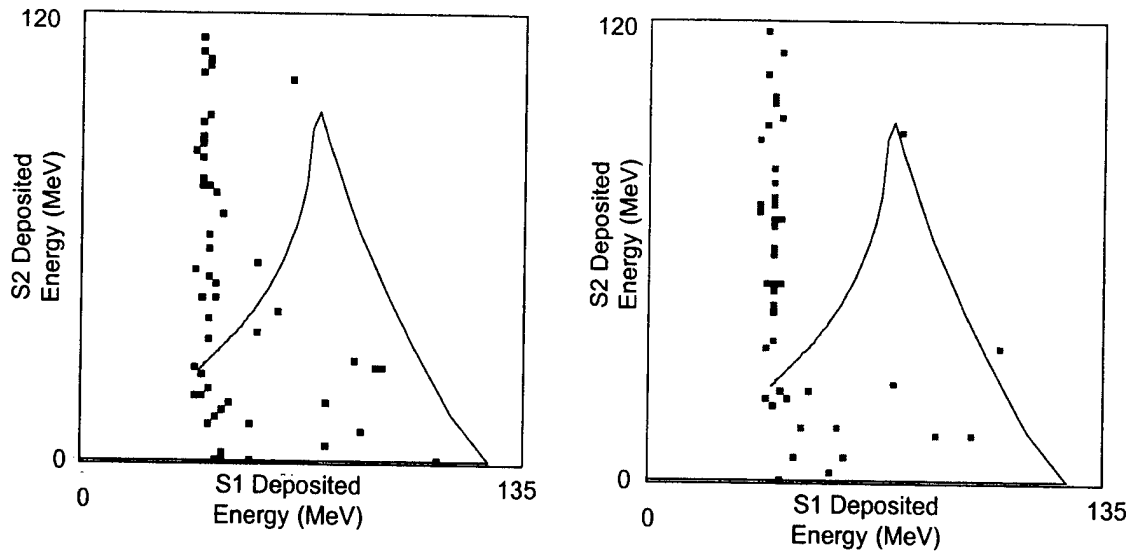


Figure 14. Measured (left) and Simulated (right) S1S2 Pulse Height Distributions for Protons Undergoing Nuclear Interactions, Incident at 250 MeV. The solid line shows the depositions predicted from the Janni model, as in Figure 3 and Figure 9. The dots are a scatter plot, showing the (S1,S2) coordinates of each event meeting the requirements discussed in the text.

The excellent agreement between the measured pattern and that predicted by the LAHET simulation code is clear. Excellent quantitative agreement was also observed between the two: the fraction of incident protons registering as valid C/D events matched that predicted by the model, to within experimental uncertainty.

#### 4 DESIGN, FABRICATION, AND TESTING OF HEP DIGITAL ELECTRONICS

The second major task of the fourth year was the design of the electronics box. The overall requirements were developed in the third year and presented in the previous annual report. Calibration of the protoflight sensor head led to some minor modifications to the requirements, but the overall design is unchanged.

Design and testing of the digital electronics required most of the effort related to the electronics box. The digital signal processing circuitry, which identifies valid events and bins the data into the raw data arrays, is key to instrument operation.

##### 4.1 DIGITAL SIGNAL PROCESSING DESIGN

A block diagram of the HEP digital signal electronics is shown below. The inputs to the DSP are (1) four timing signals, one from each of the D1-D4 detectors, (2) three pulse height analysis (PHA) signals from each of the D1-D4 detectors, (3) a timing signal from the S3 scintillator, (4) the analog shaped signals from the S1 and S2 scintillators, and (5) a trigger signal from the S1 and S2 scintillators. The primary output from the DSP is a set of six, 120 element histograms, each representing the number of events which (1) match one of 6 predefined patterns for the D1-D4 and S3 detectors and (2) have pulse heights in the S1 and S2 scintillators within one of 120 ranges. The secondary output is the raw count rates in all seven detectors, of electrons, and of pattern matches.

A particular pattern in the D1-D4 and S3 detectors (termed trigger detectors) is called a logic mask. For example, one could require valid, simultaneous signals in D1-D4 but no signal in S3.

There are 32 logically possible logic masks. At any one time, six patterns can be selected, commandable from the ground. Each of the 120 output channels is associated with a given set of (S1, S2) values, a region in the (S1, S2) plane, as was discussed previously. The channel numbers are associated with the two-dimensional S1S2 amplitude pattern, while the logic mask is associated with the trigger detector pattern. It is the combination of the logic masks and channel number which identifies the origin of the protons.

There are actually two different 6 x120 raw data arrays in memory. At any time, one is active (with the DSP circuitry adding counts) and the other is inactive (being read and cleared by the microprocessor). These two ping-pong at microprocessor command. The array depths are appropriate for a readout interval of approximately 100 milliseconds.

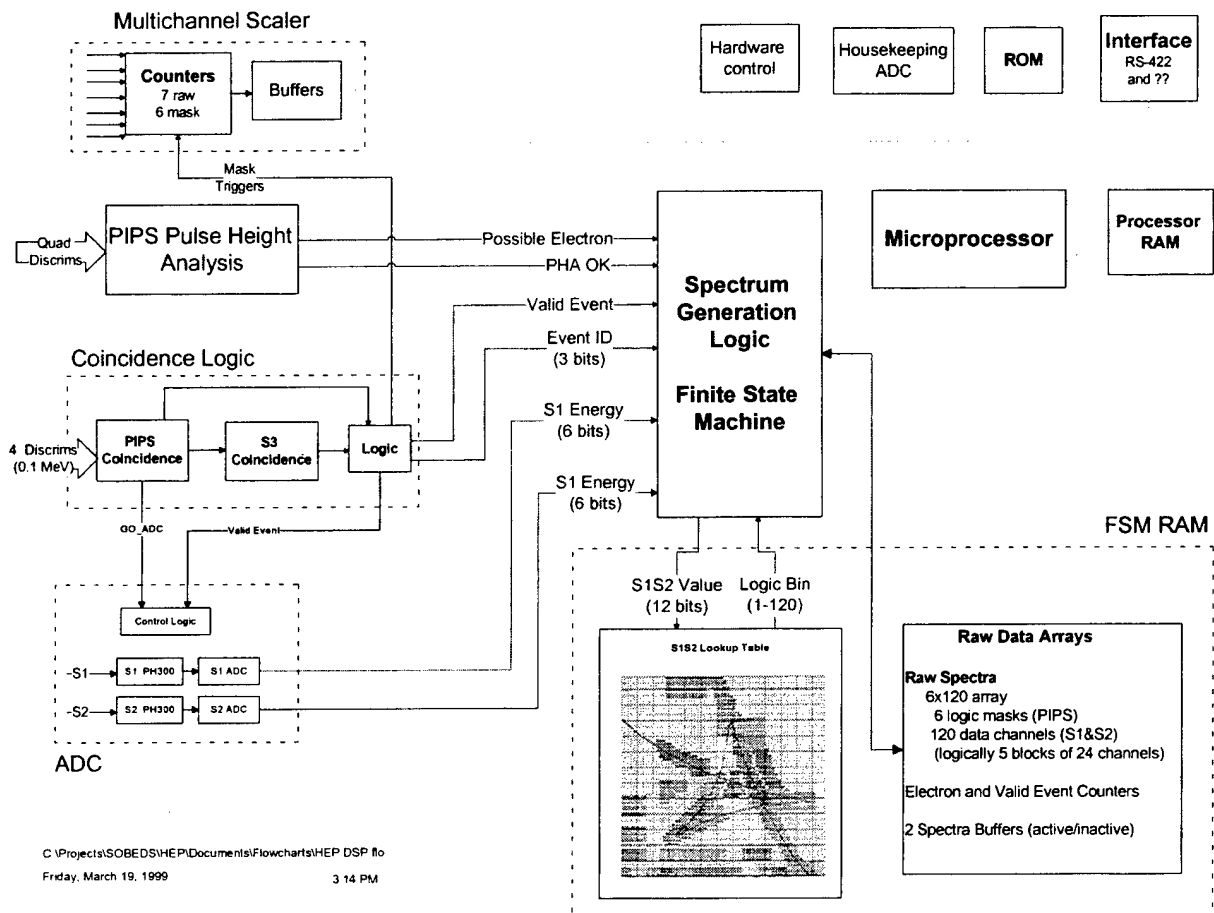


Figure 15. Simplified Block Diagram of the HEP Digital Electronics.

There are six major function blocks in the DSP circuitry: 1) the coincidence logic, 2) the PIPS Pulse Height Analysis, 3) the Analog to Digital Converter, 4) the S1S2 Lookup Table, 5) the Spectrum Generation Logic, and 6) the Multichannel Scaler.

#### *Coincidence Logic and PIPS Pulse Height Analysis*

The primary purpose of the coincidence logic is to determine if the D1-D4 and S3 detectors were triggered, within a 100 nsec timing window, with a pattern that matched one of the six defined logic masks. If there was such a match, then the rest of the processing proceeds. The coincidence logic also initiates the S1 and S2 ADC if a possible event occurs. Because the event

processing can take considerable time, if other valid events occur while an initial event is being processed, the coincidence logic identifies and counts such matches. The outputs of the coincidence logic are (1) an *Event Trigger*, signaling that a valid event occurred, (2) an *Event ID*, a three-bit value indicating which of the six logic masks was matched, (3) a *Go ADC* signal to start the S1 and S2 ADC, and (4) six *Mask Match* signals which are triggered each time one of the masks is matched.

The coincidence logic is a particularly critical portion of the digital electronics, since it controls all subsequent data processing. Requirements include a 100 nsec timing window for the PIPS detectors, stability over temperature and radiation, a separate, delayed 100 nsec timing window for S3 (due to its 200 nsec risetime), and the ability to set six different logic masks. The coincidence logic is implemented in a rad-hard FPGA, using passive delay lines to set the timing windows. The delay lines are inherently radiation hard and temperature stable, and a wide variety of delays are available to tailor the design. Moreover, they permit a completely asynchronous design with high timing accuracy, as is necessary.

The PIPS PHA was also implemented on the same FPGA. The primary purpose of the PIPS Pulse Height Analysis is to verify that the pulse heights in the D1-D4 detectors are consistent with that expected for given proton energy ranges, determined by the logic masks. The secondary purpose is to identify when the pattern of energy deposition and D1 and D2 is consistent with the energy of an energetic electron. The outputs of the PIPS PHA are (1) a *PHA OK* signal, which indicates that energy deposition is consistent with the logic mask, and (2) an *Electron* signal, indicating that energy deposition was consistent with electrons.

#### *ADC and Lookup Table*

The purpose of the Analog to Digital Converter is to digitize the S1 and S2 peak amplitudes, when a valid event occurred. The outputs of the ADC are two, six bit values, representing energy deposited in S1 and S2, respectively. For HEP, a Wilkinson type ADC was selected. It is based upon a PH300 peak-hold amplifier and a counter located in an FPGA. This provides excellent resolution and linearity, with a digitization time that varies between 1 and 6  $\mu$ sec, depending on pulse amplitude.

The purpose of the S1S2 Lookup Table is to associate the S1 and S2 amplitudes with the output channels. Each of the 120 output channels is associated with a given region in the (S1,S2) plane. The lookup table takes as input the 12 bit S1S2 value and produces as output a number from 1 to 120 indicating the output channel number. The Lookup Table is located in RAM so a new table can be uploaded during flight.

#### *Spectrum Generation Logic*

The primary purpose of the spectrum generation logic (SGL) is to produce the six, 120-element histograms from the Event ID, which indicates in which of the six histograms a particular event belongs, and from the S1S2 Lookup channel number, which indicates in which of the 120 channels a particular event belongs. The histogram is updated only if the PIPS PHA value is valid. The secondary purpose of the SGL is to identify electrons, using the combination of the Electron signal from the PIPS PHA and the output channel number. The SGL maintains two separate 6x120 arrays, one of which is active at all times. The microprocessor commands the SGL to switch buffers, reads the data out of the inactive buffer, and clears the data in the inactive buffer before switching back. The output of the SGL is the 6x120 element array.

The spectrum generation logic, implemented in an FPGA, is a finite state machine. A Valid Event Trigger from the coincidence logic interrupts the finite state machine, which then processes the data. It uses the digitized S1 and S2 amplitudes, each 6 bits long, to look up one of the 48 channels from the S1S2 lookup table which is in RAM. It then uses the 5 bit Event ID, along with the PIPS PHA results, to determine which spectrum the data go into. There are two spectrum buffers in RAM. One is active, being incremented as counts occur, while the other is inactive. The data in the inactive buffer are passed to the microprocessor, which formats the data to output to the spacecraft.

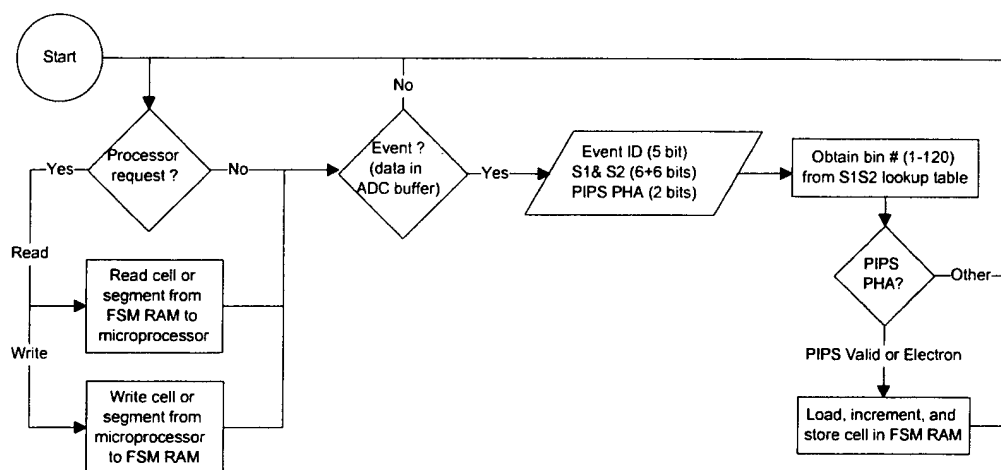


Figure 16. Block Diagram of the Spectrum Processing Logic.

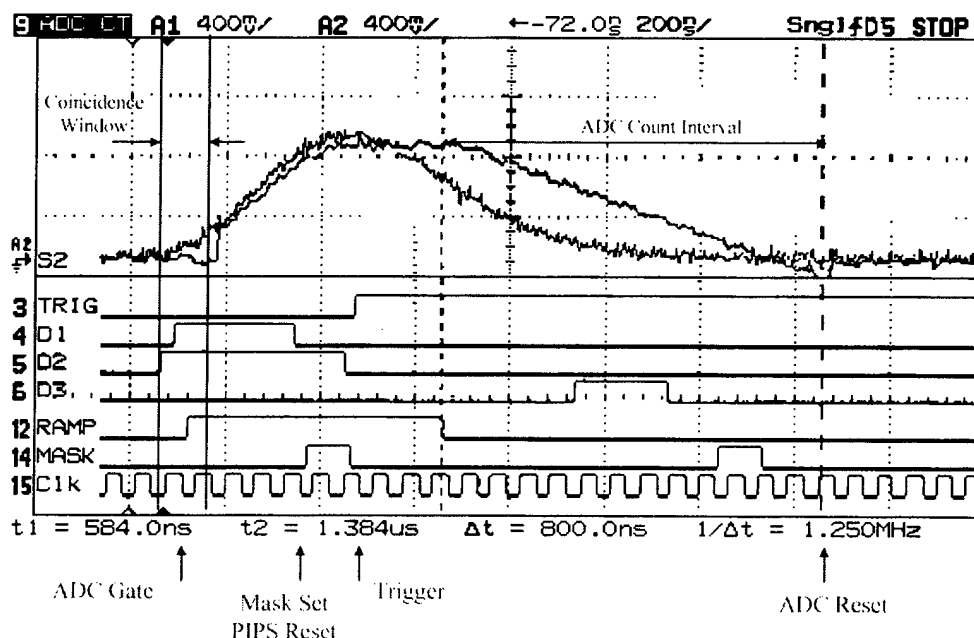


Figure 17. Timing Diagram of the DSP Circuitry, Measured With an Oscilloscope.

A timing diagram of the operation of the digital processing circuitry is shown in Figure 17, which shows measured waveforms from an oscilloscope/log analyzer. This measurement was obtained on a prototype of the complete HEP DSP using pulser inputs. The D2 signal occurs



first and starts the PIPS coincidence window, with the D1 signal occurring 25 nsec later. At the conclusion of the 100 nsec PIPS coincidence window, D1 & D2 are true, matching an "A" event which was programmed. The ADC is gated and the PH300 acquires the S2 scintillator waveform, which ramps to ground following the trigger. Both the S2 signal and the PH300 output are shown in the analog traces. The ADC counts the clock cycles between ramp initiation and the ramp zero crossing to determine the S1 amplitude.

### *Multichannel Scaler*

The purpose of the Multichannel Scaler is to count fourteen types of events. It counts the raw signal rate in each of the seven detectors, it counts the number of times each logic mask is matched, and it counts the number of times an Event Trigger is generated. Each counter has an associated latching buffer. At microprocessor command, the values are latched and then the counters are reset. The counter depths are appropriate for a 100 millisecond readout interval.

## **4.2 DIGITAL SIGNAL PROCESSING TEST AND MEASUREMENT**

In the fourth year, in addition to designing the DSP and to building prototype circuitry implemented in the FPGAs, considerable testing was carried out to verify the design. The coincidence window length was carefully measured as 100 nsec. The maximum timing walk of the PIPS signals was measured as 50 nsec. The timing jitter has a maximum 6 nsec FWHM. Timing properties were shown to change by less than 10 nsec due to changes in temperature, supply voltage and so on. The coincidence window thus has an adequate design margin.

Figure 18 shows measured accidental coincidences and vetoes, obtained using random tail pulsers. Figure 18 (a) compares the measured and computed accidental coincidence rate obtained with two random pulsers into two PIPS detectors. The accidental rate is low at the expected count rates, a few thousand counts per sec, and matches very well with that predicted for a 100 nsec window. Since HEP measures the raw rates, the accidental rate will be known and the "background" effect can be removed during data processing. Figure 18 (b) compares the measured and computed rate of false vetoes due to signals in S3. A periodic pulser was injected into D1, D2, and S1, and a random pulser into S3. At the maximum single rate expected in S3, 150,000 sec<sup>-1</sup>, the false veto rate is 15%.

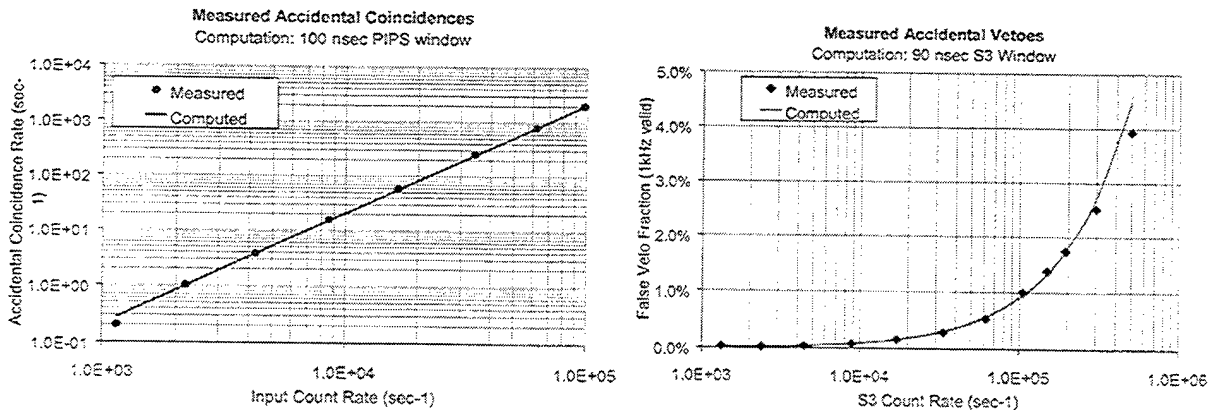


Figure 18. Plots Showing the Measured Performance of the Coincidence Circuitry. The rate of accidental coincidences and vetoes is small and matches that computed from circuit design parameters.

Figure 19 shows the performance of the multichannel scaler at high count rates. The D1, D2, D3, and D4 counter depths are based upon the maximum count rates expected in orbit, shown along the bottom axis. In each of these detectors, the observed count rate matches the input rate up to the maximum and then is flat for all higher count rates. For the scintillators, the measured count rate deviates somewhat from the input rate due to pulse pile-up. However, this deviation only occurs at count rates well above that expected on orbit ( $150,000 \text{ sec}^{-1}$ ) and is well matched by that computed from the known pulse widths.

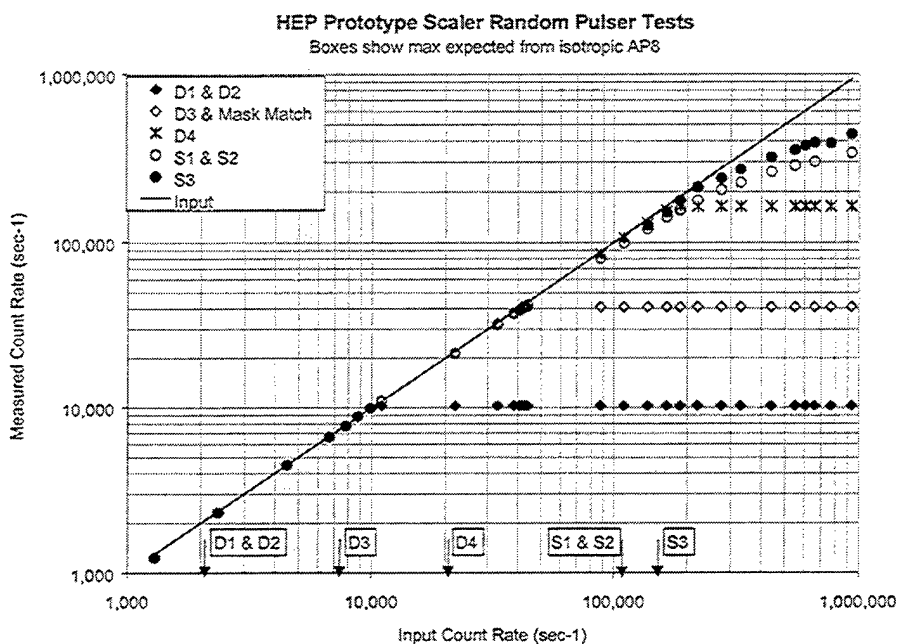


Figure 19. Measured Performance of the HEP Scalers at Count Rates up to  $10^6 \text{ sec}^{-1}$ .

Figure 20 is a plot showing the fraction of scintillator counts with distorted amplitude measurement due to pulse pile-up. This was obtained using both a random and a periodic pulser into the S1 channel. At the maximum count rate expected in S1,  $100,000 \text{ sec}^{-1}$ , about 10% of the counts yield an incorrect measured pulse amplitude. As before, this fraction is acceptably small and moreover is well matched by that expected from models. Therefore, the measurement of the raw count rate will permit correction factors to be determined on the ground using on-orbit measurements.

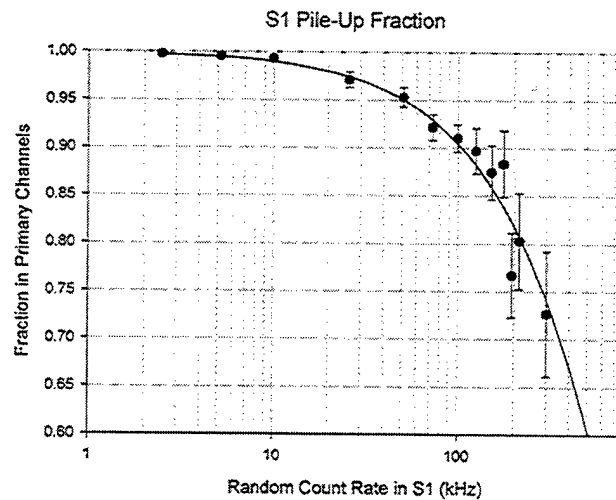


Figure 20. Plot Showing the Measured Effects of Pulse Pile-up in S1.

### 4.3 CPU AND INTERFACE DESIGN

The primary purpose of the HEP CPU is to read the data output from the DSP circuitry, to sum the selected values over a readout interval, and to log compress the summed values for telemetry. The secondary purposes of the CPU are to receive and process commands from the ground, and to handle housekeeping. In the fourth year, considerable progress has been made in designing the CPU. However, since the spacecraft has not yet been determined, there are several very important unknowns. The most important unknowns include the telemetry rate, the spin rate of the spacecraft, and the type of spacecraft interface.

A minimum HEP data packet consists of six, 24 channel spectra, the fourteen scaler values, and some housekeeping data. Assuming log compression of the spectra and scalers, this is 159 bytes (8 bits each) plus hand-shaking. To measure the pitch angle distribution of energetic protons, a complete HEP packet should be associated with each pitch angle bin. At the PDR, held in 1997, Amptek was directed by AFRL/VSBS to assume that the spacecraft had a relatively low spin rate, with a minimum data acquisition interval of 1 second, and a relatively high data rate, of one packet per second. Data would simply be acquired and then transmitted. Amptek was further directed to assume a MIL-STD-1553B interface.

During the most recent year, as spaceflight opportunities were examined, it became clear that some of the most promising opportunities did not meet these assumptions. One particular spacecraft had a spin period of 6 seconds. Since AFRL/VSBS requested a pitch angle resolution of 6 seconds, this implied an acquisition interval of 100 milliseconds. This would imply a data rate of 1,590 bytes per second, but this same spacecraft had a maximum data rate of 60 bytes per second available. Further, this spacecraft did not have any standard communications interface.

Although it is not yet known if this spacecraft will be used, a more flexible CPU and interface was clearly required, consistent with the SOBEDS goal of developing instruments flexible enough to fly on many spacecraft. This flexibility involved two key changes to the data processing requirements, defined in the previous year.

First, the CPU now has the capability of summing data over many spins. The CPU maintains up to 60 different internal pitch angle arrays. At selected time intervals, based on the spin rate and desired pitch angle resolution, raw data from the DSP are directed into the proper

pitch angle array. Data are summed in these arrays for whatever length of time is required to provide the proper average data rate. This change added considerably to the amount of memory in the CPU and to some software complexity.

Second, the CPU now has the capability to support different telemetry modes. Transmitting the complete set of spectra could take several minutes, but it is desirable to obtain a subset of the spectral data at a higher temporal resolution, to measure spatial variation in the proton population. The HEP CPU can be commanded to download various size subsets of the 6x120 array generated by the DSP.

Since the final spacecraft is not known, the software requirements cannot be fully defined. At this point, software is being written which contains the possibility of doing pitch angle binning and supporting multiple modes. Defining exactly what modes are needed must await spacecraft selection. Similarly, the CPU is now being designed to support an RS422 interface for bench testing. Design of the spacecraft interface will await spacecraft selection.

## **5 DESIGN AND FABRICATION OF OTHER HEP COMPONENTS**

### **5.1 SENSORS**

As discussed above, tests carried out on the protoflight sensor head demonstrated that the active area of the PIPS detectors exceeded that specified by the manufacturer, Canberra Inc., and that the additional area significantly degraded the angular response of HEP. Therefore, custom detectors with the correct, 25 mm<sup>2</sup> active area were purchased. These were Ultra™ passivated, ion-implanted Si detectors made by EG&G Ortec. The custom detectors were received, tested, and are used in the flight sensor head.

### **5.2 ANALOG ELECTRONICS**

In the third year, detailed design of the analog electronics was carried out. The flight preamplifier board was fabricated and tested, and has been used in the completed protoflight sensor head. A breadboard prototype of the amplifier board, which will be located in the electronics box, was fabricated and was used in the beam testing discussed above.

The breadboard circuitry developed in the third year was based on commercial-grade electronic components. In the fourth year, the flight analog electronics were developed. This involved some redesign and testing for the flight-rated amplifiers, layout of a prototype board with the footprint of the flight board, testing of the prototype board, minor modification to schematic and layout, and then fabrication of the flight board. The schematics are essentially the same as those shown in the previous annual report.

### **5.3 POWER SUPPLY**

During the fourth year, detailed design of the power supply was initiated. From the prototype analog and DSP circuitry, the power supply requirements were generated. A table of the requirements, and a comparison with the estimate given previously at the PDR, is shown in

Table 2. Based on these requirements, the circuit design was begun. The HEP power supply is similar in principle to that used in the LEPDOS instruments, but with important differences to provide the  $\pm 6V$  required for the HEP's low noise analog electronics.

Table 2. HEP Power Estimate.

		Best Case Low rate, RS422	Worst Case High rate, 1553B	PDR Estimate 11/6/97
Preamp & Amps	***	0.9	0.9	1.0
DSP	***	0.5	0.5	0.5
CPU	***	0.2	0.2	0.4
HVPS		0.1	0.1	0.1
LVPS		0.3	0.3	0.5
Subtotal		2.0	2.0	2.5
I/O		0.1	2.5	1.5
<b>Total</b>		<b>2.0</b>	<b>4.5</b>	<b>4.0</b>

All quantities in watts

\*\*\* Measured with prototypes

## 5.4 MECHANICAL DESIGN

Little change was made to the mechanical design of HEP in the past year. The flight sensor head mechanical components were designed and obtained in the third year and are discussed in the previous annual report. Fabrication drawings of the electronic box were prepared but fabrication has not yet begun. A mass estimate is given in Table 3.

Table 3. HEP Mass Estimate (in grams).

Detectors	175
Collimator	60
Shielding (Cu)	685
Boards and Connectors	120
Sensor Head Box	415
<b>Sensor Head Total</b>	<b>1,455</b>
 Sensor Head	 1,455
Electronics Box	900
Cable (2 feet))	200
<b>HEP Total</b>	<b>2,555</b>

## 6 LEPDOS DESIGN AND FABRICATION

### 6.1 DESIGN, FABRICATION, AND CALIBRATION OF STANDARD LEPDOS UNITS

One primary technical effort on LEPDOS in this fourth year of the SOBEDS contract was the fabrication and testing of two flight LEPDOS instruments. One flight instrument, S/N 004, was designed and completely fabricated during the third year of the contract. This instrument was designated for flight on the SBIRS LADS spacecraft. Meeting the SBIRS LADS schedule required extremely ambitious design and fabrication efforts. During the fourth year, the interface

was customized for this spacecraft, functional test was completed, calibration was carried out, and spacecraft specific environmental tests were carried. Shortly before this instrument was delivered, the SBIRS LADS spacecraft mission was cancelled. This instrument is now in storage at Amptek. When a new spacecraft is selected, the interface will again be customized and the testing repeated. A second flight instrument, S/N 005, has been partially fabricated. It is identical in design to the completed unit.

In addition, a calibration of the LEPDOS telescope was performed at the Van de Graaf accelerator at Goddard Space Flight Center. The response of the telescope to electrons ranging from 175 to 1,600 keV was measured. Very good agreement with model predictions was observed.

## **6.2 DESIGN, FABRICATION, AND CALIBRATION OF LEPDOS WITH ESA**

A second major technical effort on LEPDOS in the fourth year of the SOBEDS contract has been the design of a LEPDOS instrument customized for flight in geostationary orbit. SCATHA data indicated that spacecraft surface charging in geostationary orbit is due primarily to electrons with energies of 20 to 50 keV, with some charging due to lower energy electrons. The standard LEPDOS instruments do not directly measure the particle flux below 50 keV, but extrapolate from higher energies. The modified LEPDOS instrument includes an electrostatic analyzer (ESA) to measure directly measure the lower energy electron population, with energy below the threshold of the standard LEPDOS sensors. This instrument, S/N 007, has been designated for flight on one of the Defense Support Program (DSP) spacecraft.

In the fourth year of this program, a prototype ESA was designed, built, calibrated, and the data analyzed. Based on these data, the flight ESA was designed, build, and calibrated. The rest of the LEPDOS instrument was also built. Several boards were unchanged, but a completely new CPU board was required to process data from the ESA, along with new onboard data processing algorithms. Because the DSP spacecraft has unique power and telemetry requirements, extensive spacecraft specific design efforts were needed. A custom telemetry interface board was designed and built, and custom power relay box was designed, built, and tested. As the fourth year ends, the complete flight instrument S/N 007 has been fabricated, calibrated, tested, and is awaiting delivery.

### *ESA Design*

A drawing and photograph of LEPDOS with an ESA is shown in Figure 21. The ESA measures electrons with energies between 5 keV and 50 keV. It has an integrated angular response, relying on the isotropy of the electron population at geostationary altitudes for accurate measurements. The spectral data from the ESA are used by the LEPDOS processing algorithm to set the Surface Charging Hazard Register and associated Warning Flag. A select set of spectral data will be available in the Science Telemetry Packet and in a History Data Channel. The ESA is a modular design, which simply attaches to the side of the existing LEPDOS instrument. Few changes are required to LEPDOS: adding a connector and some counters and control logic. All of the necessary electronics, including the HV supply, are contained within the ESA on the side. This greatly simplifies the manufacturing of both standard and enhanced instruments.

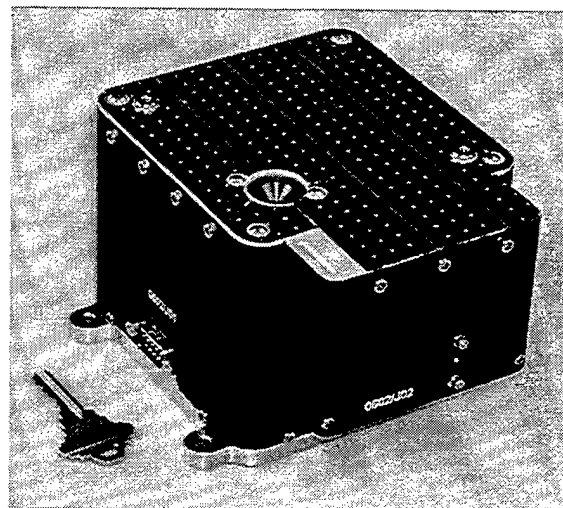
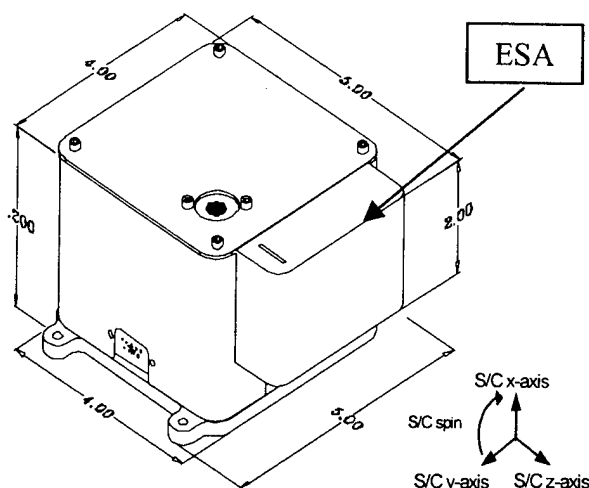


Figure 21. Drawing and Photograph of LEPDOS S/N 007, Which Includes an ESA.

Based on considerable design analysis conducted in this previous year, the basic ESA design is that of a cylindrical  $125^\circ$  ESA with a channel electron multiplier (CEM) for the sensor. This design was selected because it has significant flight experience, is straightforward to fabricate, and the performance is quite suitable for the anticipated environment. It can support a pass band from 500 eV to 50 keV, although for this particular mission the low energy cut-off was set to 5 keV.

The electronics in the ESA module include an amplifier with comparator, a customized A111F hybrid from Amptek. The ESA module also includes the HV power supply required to bias the ESA deflection plates and the CEM. A single-ended HV supply is used to simplify the design. The ESA sweeps once per second, with an exponential decay from 50 keV to 5 keV. The counts from the ESA are acquired in 25 msec bins over this energy range. The energy range is binned in 39 log-spaced steps, with the 40th bin corresponding to High Voltage Flyback. To process the data from the ESA, a counter in the CPU FPGA accumulates the counts, which are summed for the five 1 second ESA sweeps in each SDI. The summed counts for each of the 40 bins (flyback included) are then log compressed and placed in the ESA telemetry packet. The performance of the design in the anticipated geostationary orbit was modeled to verify that the worst case environment will not swamp the electronics and the minimum environment will be accurately measured.

#### *ESA Test and Calibration*

Both prototype and flight ESAs underwent extensive tests and calibrations in the MUMBO electron beam system at AFRL/VSBS. These tests validated the design, in particular the geometric factor and energy resolution and demonstrated UV rejection. Geometric calculations carried out prior to the tests predicted an energy-dependent geometric factor of  $2.9 \times 10^{-3} \text{ cm}^2\text{-ster-eV}$  at 1 keV. The experimentally measured value was  $3.1 \times 10^{-3} \text{ cm}^2\text{-ster-eV}$ , in excellent agreement. The measured focused and unfocused angular responses were  $2^\circ$  and  $8^\circ$  FWHM, again in good agreement with the results of the calculations. The measured geometric factors and energy bins boundaries are shown in Table 4.

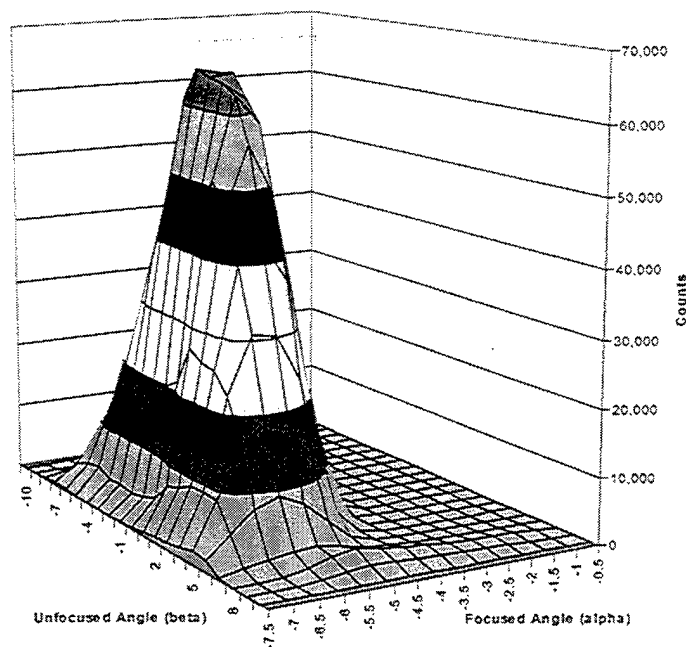


Figure 22. Plot Showing the Measured Angular Response of the ESA. The angular resolution is  $2^\circ$  FWHM in the focused direction and  $8^\circ$  in the unfocused direction.

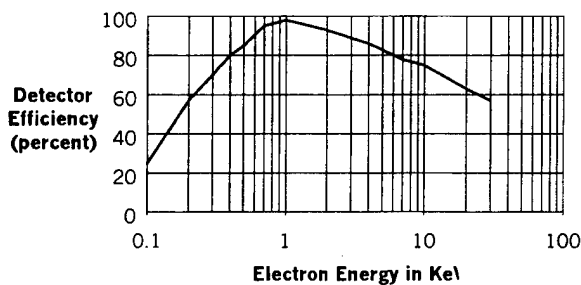
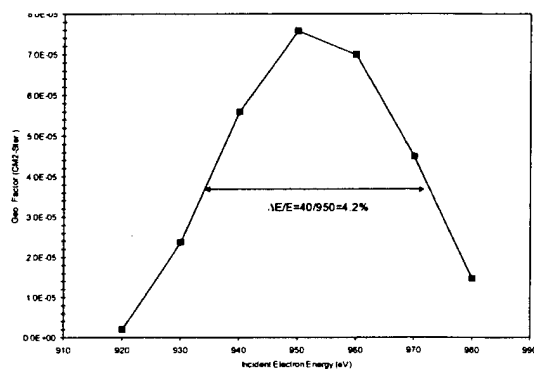


Figure 23. Left: Plot Showing the Measured Energy Passband at 1 keV. The energy resolution is 4.2% FWHM, and the geometric factor is  $3.1 \times 10^{-3} \text{ cm}^2\text{-ster-eV}$ . Right: Plot Showing the Measured Efficiency of the CEM as a Function of Incident Energy.



Table 4. Measured Energy Bins, Boundaries, and Geometric Factors for the LEPDOS ESA.

ESA Bin	GFs (cm <sup>2</sup> -sec-sr-eV)	Center Energy (eV)	Bin Boundaries (eV)	
			Upper	Lower
0	1.02E-01	49,271	50,749	47,793
1	1.12E-01	46,351	47,741	44,960
2	1.13E-01	43,604	44,912	42,296
3	1.13E-01	41,020	42,250	39,789
4	1.13E-01	38,588	39,746	37,431
5	1.13E-01	36,301	37,390	35,212
6	1.12E-01	34,150	35,175	33,126
7	1.11E-01	32,100	33,063	31,137
8	1.10E-01	30,200	31,106	29,294
9	1.08E-01	28,400	29,252	27,548
10	1.06E-01	26,700	27,501	25,899
11	1.04E-01	25,125	25,879	24,371
12	1.02E-01	23,625	24,334	22,916
13	9.99E-02	22,250	22,918	21,583
14	9.77E-02	20,950	21,579	20,322
15	9.54E-02	19,700	20,291	19,109
16	9.29E-02	18,510	19,065	17,955
17	9.03E-02	17,435	17,958	16,912
18	8.79E-02	16,450	16,944	15,957
19	8.56E-02	15,475	15,939	15,011

ESA Bin	GFs (cm <sup>2</sup> -sec-sr-eV)	Center Energy (eV)	Bin Boundaries (eV)	
			Upper	Lower
20	8.31E-02	14,550	14,987	14,114
21	8.05E-02	13,675	14,085	13,265
22	7.79E-02	12,875	13,261	12,489
23	7.54E-02	12,125	12,489	11,761
24	7.30E-02	11,425	11,768	11,082
25	7.06E-02	10,775	11,098	10,452
26	6.84E-02	10,145	10,449	9,841
27	6.60E-02	9,550	9,837	9,264
28	6.37E-02	9,000	9,270	8,730
29	6.15E-02	8,480	8,734	8,226
30	5.93E-02	7,985	8,225	7,745
31	5.72E-02	7,520	7,746	7,294
32	5.51E-02	7,075	7,287	6,863
33	5.30E-02	6,660	6,860	6,460
34	5.09E-02	6,275	6,463	6,087
35	4.90E-02	5,915	6,092	5,738
36	4.72E-02	5,575	5,742	5,408
37	4.45E-02	5,255	5,413	5,097
38	4.19E-02	4,955	5,104	4,806
39	Flyback			

#### Data Processing Hardware and Software

The ESA data are binned into 40 bins, summed for 5 seconds. The onboard data processing software places these values directly into the ESA Science Data packet, and also sums them to generate the Surface Dielectric Charging Status Register and Warning Flag.

For the Science Data packet, the data are log compressed (6-bit mantissa, 2 bit exponent) into one byte. The compression scheme has been chosen to accommodate expected flux levels, using SCATHA worst case instantaneous count rates and accumulating over 5 seconds in a given energy interval. To reconstruct from the telemetry the Counts/Bin summed over the SDI for one of the 40 intervals, use the following equation:

$$\text{Counts/Bin Summed over SDI} = ((M + 64.5) * 2^E) - 64$$

where  $M$  is the mantissa and  $E$  is the exponent.

In this fourth year, a new the LEPDOS processing algorithm was developed to use the spectral data from the ESA to set the Surface Charging Hazard Register and associated Warning Flag. The measured count rate, for some actual incident directional differential number flux  $J(E)$ , in units of electrons/cm<sup>2</sup>-sec-ster-eV, is given by:

$$CR_{\text{meas}}(E) = J_{\text{actual}}(E) * GF * \delta E(E) * \epsilon(E) \quad \left( \frac{\text{elec}}{\text{sec}} \right) = \left( \frac{\text{elec}}{\text{cm}^2 - \text{sec} - \text{ster} - \text{eV}} \right) (\text{cm}^2 \text{ster}) (\text{eV}) (\text{unitless})$$

where GF is the energy independent geometric factor,  $\delta E$  is the energy resolution of the ESA, and  $\epsilon(E)$  is the efficiency. We can combined these three terms into the energy dependent geometric factor,  $GF(E) = GF * \delta E * \epsilon(E)$  in units of  $\text{cm}^2\text{-ster-eV}$ . This expression can obviously be inverted to obtain the directional differential number flux,

$$J_{\text{meas}}(E) = CR_{\text{meas}}(E) / GF(E)$$

The incident directional number flux over an energy range equals:

$$J_{\text{int}} = \int_{E_{\min}}^{E_{\max}} J(E) dE = \sum_{i_{\min}}^{i_{\max}} J_{\text{meas}}(E_i) \Delta E_i = \sum_{i_{\min}}^{i_{\max}} \frac{CR_i}{GF(E_i)} \Delta E_i$$

where the *Incident Flux*  $J$  is in units of *electrons/cm<sup>2</sup>-sec-sr*,  $CR$  is in *counts/sec*,  $E$  in *eV*, and  $GF$  in *cm<sup>2</sup>-sec-sr-eV*. and where  $i$  corresponds to sweep energy step,  $n \geq 0$ ,  $E_n \equiv E_{\min}$ ,  $E_0 = 50$  keV, and  $GF$  are the energy dependent weight factors. Note that the sum is taken over the energy sweep with bin widths of  $\Delta E$ .

Parameter  $E_{\min}$  is the selected minimum electron energy that contributes to spacecraft charging. The default for CEASE II will be  $E_{\min} = E_{26} = 10$  keV. Additional  $E_{\min}$  choices available through ground commanding will be: 5, 20 and 30 keV. The weighting factors  $GF$  account for: 1) sensor detection efficiency, 2) energy channel width, and 3) sensor geometry. These factors have been determined from the ESA calibration discussed previously.

Surface dielectric charging (SDC) is the charging of externally located spacecraft dielectric surfaces by low energy electrons. By definition, the electrons responsible for SDC have very short ranges in typical spacecraft materials. Therefore, the incident flux of interest is  $\frac{1}{2}$  of the omni-directional flux since the spacecraft body, or other instruments, will shield the "back" side of the surface. The Effective Surface Charging Flux ( $F_{\text{SDC}}$ ) in an EMI, in units of *electrons/cm<sup>2</sup>-sec*, is then:

$$F_{\text{SDC}} = 2\pi \int_{E_{\min}}^{E_{\max}} J(E) dE = \frac{2\pi}{\Delta T} \left\{ \sum_{i_{\min}}^{i_{\max}} \frac{CTS_i}{GF * \delta E(E_i) * \epsilon(E_i)} \Delta E_i \right\} = \left( \frac{2\pi}{\Delta T} \right) \left\{ \sum_{i_{\min}}^{i_{\max}} \frac{\left[ \sum_{j=1}^{60} RAW\_CTS_{ij} \right]}{GF * \delta E(E_i) * \epsilon(E_i)} \Delta E_i \right\}$$

where  $\Delta T$  is the total time that each bin is measured in an EMI,  $\Delta T = 0.025 \text{ sec} * 60 \text{ sweeps} = 1.5 \text{ sec}$ . Above a threshold,  $B_7$ , for  $F_{\text{SDC}}$ , charging can be designated a hazard. The Surface Charging Hazard Register ( $HR_7$ ) is a measure of the hazardous flux of low energy electrons. To compute  $HR_7$ , we define an array  $G_i$  for each  $B_7$ , and compute:

$$G_i = \left( \frac{2\pi}{\Delta T} \right) \left( \frac{\Delta E_i}{GF * \delta E(E_i) * \epsilon(E_i)} \right) \left( \frac{1}{B_7} \right) = \left( \frac{2\pi}{\Delta T} \right) \left( \frac{\Delta E_i}{GF(E_i)} \right) \left( \frac{1}{B_7} \right),$$

$$\frac{F_{\text{SDC}}}{B_7} = \sum_{i_{\min}}^{i_{\max}} \left[ G_i \left( \sum_{j=1}^{60} RAW\_CTS_{ij} \right) \right]$$

Threshold values for  $HR_7$  are 0-15.  $HR_7$  is computed as follows:

$$HR_7 = 3 * \log_{10} (F_{SDC} / B_7)$$

When the calculated  $HR_7$  exceeds its threshold value for 3 consecutive EMI, the Warning Flag is set. The default  $HR_7$  threshold value is 15.

#### *Summary*

A flight LEPDOS instrument, customized for the geosynchronous orbit by including an ESA to measure charging, was designed, built, and calibrated. This required the design of a suitable small, lower power ESA and the development of software for autonomous data processing. In addition, because of the unique requirements of the DSP spacecraft, a custom interface board and a custom power relay box were designed, built, and tested. The complete flight instrument is awaiting delivery.